

## Boson peak and terahertz frequency dynamics of vitreous silica

This article has been downloaded from IOPscience. Please scroll down to see the full text article.

2002 Rep. Prog. Phys. 65 1195

(<http://iopscience.iop.org/0034-4885/65/8/203>)

View [the table of contents for this issue](#), or go to the [journal homepage](#) for more

Download details:

IP Address: 193.174.246.175

The article was downloaded on 25/06/2012 at 16:16

Please note that [terms and conditions apply](#).

## **Boson peak and terahertz frequency dynamics of vitreous silica**

**Tsuneyoshi Nakayama**

Department of Applied Physics, Hokkaido University, Sapporo 060-8628, Japan

Received 16 April 2002, in final form 9 July 2002

Published 29 July 2002

Online at [stacks.iop.org/RoPP/65/1195](http://stacks.iop.org/RoPP/65/1195)

### **Abstract**

This paper describes the progress that has been made in the past decade in the investigation of the peculiar dynamic properties of vitreous silica ( $v\text{-SiO}_2$ ) and related glasses in the terahertz (THz) frequency range. The reason why we focus our attention on  $v\text{-SiO}_2$  is that it is one of the principal network glasses and exhibits all features typical of glasses. These are the increased inelastic scattering of light and neutrons at THz frequencies, the so-called Boson or Bose peak, as well as unusual thermal properties such as specific heats and thermal conductivities at low temperatures. During the last decade, experimental techniques such as the inelastic scattering of light, neutrons and x-rays have been greatly improved, and these have provided considerable experimental information about the atomic vibrations in  $v\text{-SiO}_2$  and related glasses in the THz frequency region. In addition, molecular dynamics simulations have proved successful for these complex systems. They form the basis for this perspective on the major advances in this decade from a new and tutorial point of view.

## 1. Introduction

### 1.1. Brief history

Glasses behave in a way that is strikingly different in the terahertz (THz) frequency range from conventional disordered systems. The history of the research is relatively old. The first and perhaps obvious anomaly in glasses was discovered almost half a century ago by Berman (1949, 1950), who noticed the unexpected instance of the thermal conductivity anomaly for vitreous silica ( $v\text{-SiO}_2$ ). He measured the thermal conductivities of several samples of  $v\text{-SiO}_2$  in the temperature range between 2.2 and 90 K and found the plateau behaviour of thermal conductivities at around 10 K with a magnitude *several orders* smaller than those of crystals. However, these properties attracted little attention until the work by Zeller and Pohl (1971).

Another important observation was made as early as the 1950s by Krishnan (1953) during his experimental investigation on Raman scattering (RS) for  $v\text{-SiO}_2$ . He found for  $v\text{-SiO}_2$  a broad band in the vicinity of  $30\text{--}120\text{ cm}^{-1}$  (note that  $1\text{ THz} = 33.35\text{ cm}^{-1}$ ) which markedly differs from the behaviour of crystals. Figure 1 shows his photographed result obtained using  $2536\text{ cm}^{-1}$  radiation of mercury as the exciter, which recovers all of the main features of the RS for  $v\text{-SiO}_2$  observable by modern laser spectroscopy such as a broad band in the vicinity of  $30\text{--}120\text{ cm}^{-1}$  and a second broad band at  $430\text{ cm}^{-1}$  in addition to the sharp  $D_1$  and  $D_2$  defect lines at  $495$  and  $606\text{ cm}^{-1}$  (Winterling 1975, Galeener and Lucovsky 1976). The defect lines  $D_1$  and  $D_2$  are assigned today as the symmetric breathing mode of 4-membered and 3-membered ring structures, respectively (Bell *et al* 1968, Galeener and Mikkelsen 1981, Galeener *et al* 1984, Galeener 1982, Pasquarello and Car 1998, Uchino *et al* 1998, 2000). Krishnan (1953) noted in his paper that *the most important new result is the appearance of a broad and intense band at  $30\text{--}120\text{ cm}^{-1}$* . This band has its maximum intensity at the low frequency end and the intensity falls off continuously. Since the temperature dependence of the intensity follows that of a harmonic oscillator characterized by the Bose factor, this has to be called the *Boson* or *Bose peak*.

The universal features of the thermal properties in glasses in the THz frequency range and below have been discovered for a variety of glasses (Zeller and Pohl 1971, Zatlin and Anderson 1975, Freeman and Anderson 1986). These are the specific heat linear in temperature  $T$  below a few Kelvin, the plateau of the thermal conductivity  $\kappa(T)$  at around 10 K, and the subsequent rise at the high-temperature end of the plateau at  $10\text{--}30\text{ K}$  (figure 2). The low-temperature thermal expansion coefficient was also shown to have an anomalous temperature dependence (Ackerman and Anderson 1982, Wright and Phillips 1984). These experimental results for specific heat and thermal conductivity, in particular, show a most remarkable universality which appears to be insensitive to the chemical composition of glasses, especially for strong and intermediate glasses in the sense of the classification by Angell (1995).

As far as the low-temperature problem observed below 1 K is concerned, the tunnelling or two-level-system (TLS) model has been most successful (Anderson *et al* 1972, Phillips 1972). In this model, atoms or groups of atoms occupying one of two adjacent minima are postulated to tunnel quantum-mechanically to the other, leading to a splitting of the ground state. To recover the observed low-temperature properties of glasses from such a model, one has to postulate that the distribution of these TLS is uniform, independent of the splitting between two low-lying energy states. The interactions between TLS had been considered negligible at the temperature at which experiments are performed. See, for example, a review by Phillips (1987). At millikelvin (mK) temperatures, however, the frozen-in state of the TLS should be realized via elastic or electric dipole interactions between TLS, which yield different features in thermal properties from those observed in the temperature range  $0.1\text{--}1\text{ K}$

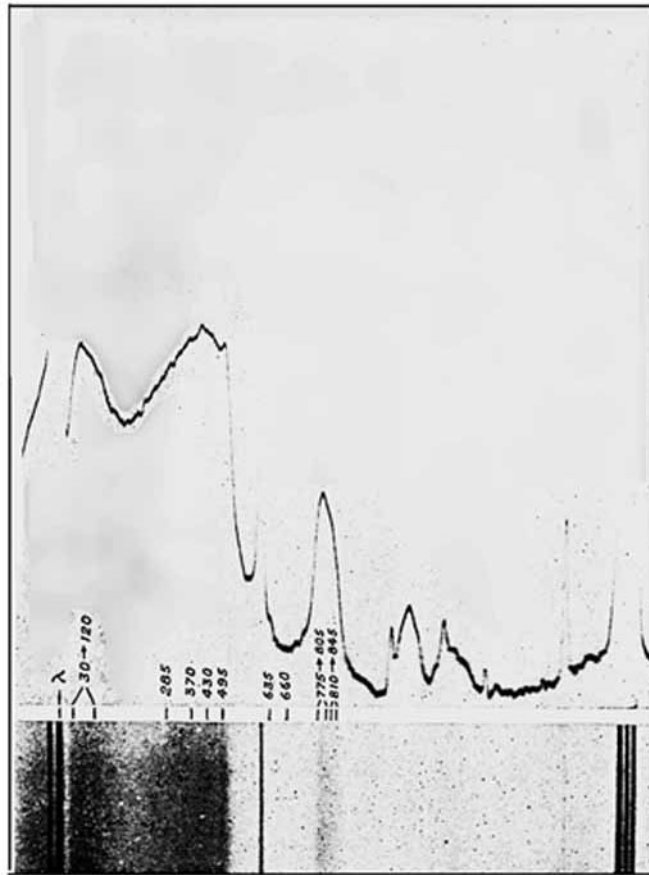


Figure 1. Raman spectrum of v-SiO<sub>2</sub>. After Krishnan (1953).

(Yu and Leggett 1988, Grannan *et al* 1990). In this temperature range, investigations on TLS in glasses seem to be entering a new stage in the past few years since experiments at very low temperatures around 1 mK present new unexpected phenomena (Rogge *et al* 1996, 1997a, 1997b, Strehlow *et al* 1998, Hunklinger *et al* 1999, Kettemann *et al* 1999, Wohlfahrt *et al* 2001, Ludwig *et al* 2002, Würger 2002).

### 1.2. Purpose of this paper

The Boson peak refers to an excess contribution to the usual Debye density of states (DOS) observed by a variety of optical, neutron, and thermal measurements in the THz frequency range. The broad peaks are in fact observed in almost all glasses at frequencies about 10–100 times smaller than the corresponding Debye frequency  $\omega_D$ . This definition of the Boson peak, however, is *not sufficient* to emphasize the peculiarity of the corresponding vibrational states, because there are a lot of non-glassy materials showing an *excess* DOS at  $\omega/\omega_D \approx 10^{-1}$ – $10^{-2}$  (Leadbetter 1969, Caplin *et al* 1973, Bilir and Phillips 1975), indicating that the comparison with only the Debye DOS as a base line is generally unjustified. As typical examples, we note the experimental work of Bilir and Phillips (1975), who showed that the specific heat of  $\alpha$ -cristobalite is not significantly different from that of v-SiO<sub>2</sub>, and similarly for neutron

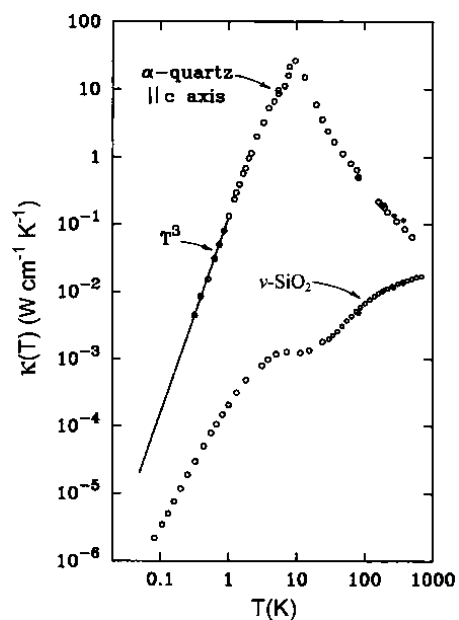


Figure 2. Thermal conductivities  $\kappa(T)$  for  $v\text{-SiO}_2$  and  $\alpha\text{-quartz}$ . After Cahill and Pohl (1987).

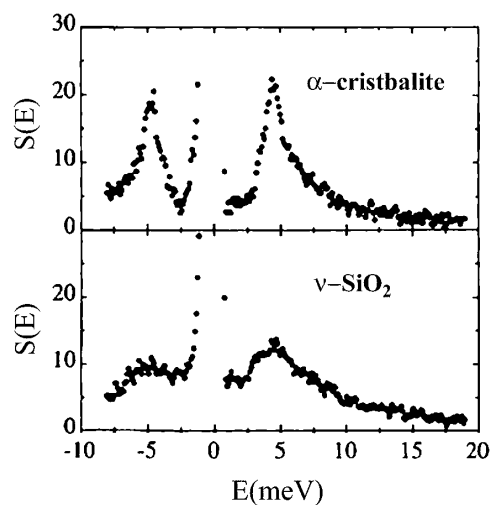


Figure 3. Inelastic neutron scattering (INS) at energies  $E = 5$  meV for  $\alpha\text{-cristobalite}$  and  $E = 4.5$  meV for  $v\text{-SiO}_2$ . After Dove *et al* (1997).

scattering data for  $\alpha\text{-cristobalite}$  and  $v\text{-SiO}_2$  by Leadbetter (1969) and Dove *et al* (1997) as shown in figure 3. Thus, it is not sufficient to explain only one aspect of the dynamics of glasses, for example, *the excess DOS* observed at THz frequencies, in order to elucidate the physical origin of the anomalous behaviour observed in the THz frequency region.

At first glance, the physical origin of the anomalous properties observed in the THz frequency range in glasses seems not to be so complicated in comparison with that of the

quantum-mechanical low-temperature anomaly below a few Kelvin. However, no satisfactory model has been proposed to interpret a wide variety of the phenomena observed in the THz frequency range in a consistent way, indicating the complexity of the physics involved. In fact, theoretical studies have not, until recently, provided a real understanding of the physical origin of the THz frequency dynamics in glasses. The main difficulty arises from the fact that, though a crystal possesses a single potential minimum yielding specific dynamic properties, a glass is characterized by a potential function with many local minima.

This paper deals with the investigations to elucidate the physical origin of the Boson peak and related phenomena observed in the THz frequency range, as well as the anomalous thermal properties such as phonon transport observed in a wide temperature range (Zeller and Pohl 1971). v-SiO<sub>2</sub> is one of the principal network glasses (that is, covalently bonded) and exhibits all the main features that are typical of glasses. For this reason, this paper treats v-SiO<sub>2</sub> and related network glasses. Though several review articles have been recently published on this subject (see, e.g. Buchenau 2001, Ruocco and Sette 2001), this paper is organized under different and more general points of view.

## 2. Structures of v-SiO<sub>2</sub> at atomic scales

### 2.1. Various phases of silica

Glasses, obtained by rapid cooling of corresponding liquid states, exhibit a large change of specific heat at the glass transition temperature  $T_g$ , and the entropy difference between a glass and the corresponding crystal below  $T_g$  remains approximately constant (see, e.g. Schulze 1990). Thus, glasses definitely possess zero-point entropies  $S_0$  (finite entropies as  $T \rightarrow 0$ ) originating from quenched disorder in the low-temperature state. A simple analysis for v-SiO<sub>2</sub> using the relation  $S_0 = k_B \ln W$  suggests that there are of the order of  $W \approx 2^N$  metastable states denoted by two-site potentials, where  $N$  is the number of SiO<sub>4</sub> tetrahedra (Schulze 1990). Such large zero-point entropies have been observed in many types of glasses. The existence of zero-point entropy is a hallmark of glasses.

Silica possesses a rich phase consisting of infinite network structures of SiO<sub>4</sub> tetrahedra connected by oxygen (O)-atoms. The shape of tetrahedra is quite rigid and not sensitive to the condition of preparation, with the Si–O distance of  $1.61 \pm 0.01$  Å. v-SiO<sub>2</sub> differs from its crystalline forms in only one aspect, namely, *the tetrahedra are randomly oriented* with a broad distribution of Si–O–Si angles around 145°, with bond angle fluctuations of about 25° as suggested from the analysis of diffraction data (Mozzi and Warren 1969, Guissani and Guillot 1996) and from nuclear magnetic resonance (NMR) studies (Devine *et al* 1987, Neufeind and Bunsenges 1996). Various anomalous structural behaviours are observed in v-SiO<sub>2</sub> such as a softened structure under hydrostatic pressure (Bridgman 1948) and negative thermal expansion (Gibbons 1959). These anomalous features are associated with the distribution of bent Si–O–Si configuration (Vukcevich 1972). However, there definitely exists medium-range order (MRO) (Elliott 1991) in v-SiO<sub>2</sub>, as confirmed by diffraction experiments (Phillips 1981, Moss and Price 1985, Wright *et al* 1985, Chervinka 1987, Fowler and Elliott 1987, Wright *et al* 1991, Suzuya *et al* 2000, Kohara and Suzuya 2001), which imply the existence of pseudo-periodicity characterized by the scale of the first sharp diffraction peak (FSDP) appearing at the wave number  $Q_1 = 1.51$  Å<sup>-1</sup>. The distance characterizing MRO is estimated as  $R_1 = 2\pi/Q_1 \approx 4.2$  Å found from the position of the FSDP at  $Q_1 = 1.51$  Å<sup>-1</sup> (see figure 4). The distance  $R_1$  is close to the average height of  $d_1 \approx 4.1$  Å of ‘SiSi<sub>4</sub>’ tetrahedra decorated with O-atoms (see figure 5), namely, the (111) spacing in crystalline silica and cristobalite. Figure 4 shows the neutron diffraction data various densities of v-SiO<sub>2</sub>, exhibiting the FSDP

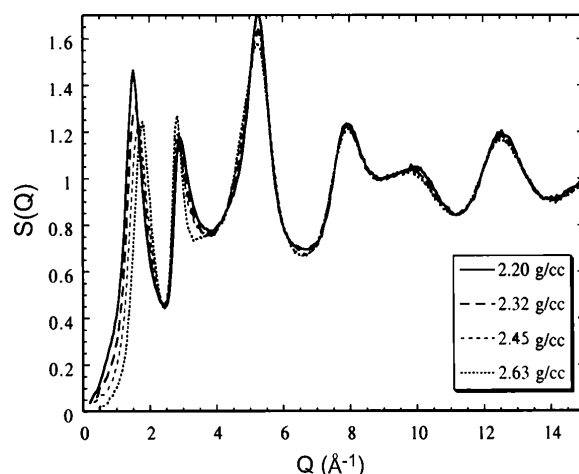


Figure 4. Neutron diffraction data for various densities of  $v\text{-SiO}_2$ . After Inamura *et al* (2001).

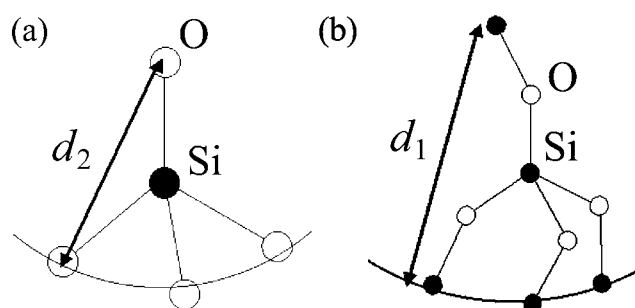


Figure 5. Possible assignment of the typical length scales. (a)  $d_2$  represents the length scale between O-atoms. (b)  $d_1$  does the length scale of the correlation between Si-Si next nearest neighbours. After Taraskin and Elliott (1998).

and subsequent peaks. The FSDP may correspond to the average height of ‘ $\text{SiSi}_4$ ’ tetrahedra decorated with O-atoms as depicted in figure 5 (Taraskin and Elliott 1998).

The equilibrium sequence of phase transitions of *crystalline* states of silica, prior to melting at 2000 K, is, first,  $\alpha$ -quartz to  $\beta$ -quartz (via an incommensurate phase at 847.3 K), then to HP-tridymite (940 K), and finally to  $\beta$ -cristobalite (1743 K) (see, e.g. Aoki *et al* 2000). The kinetics of these phase transitions can be extremely sluggish, and there are several other metastable crystalline phases of lower symmetry derived from cooling HP-tridymite and  $\beta$ -cristobalite. An example is  $\alpha$ -cristobalite obtained from  $\beta$ -cristobalite below about 553 K (Kimizuka *et al* 2000). The structure of  $\alpha$ -cristobalite is well understood (Pluth *et al* 1985). However, there is still much discussion as to the microscopic structure of the  $\beta$ -phase. The similarity of the FSDP in  $v\text{-SiO}_2$  and  $\beta$ -cristobalite has led to the suggestion that there is a close relationship over short-length-scales between these two phases (Le Bail 1995, Gaskell and Wallis 1996, Keen and Dove 1999). Keen and Dove (1999) suggested that the instantaneous local atomic arrangements of HP-tridymite and  $\beta$ -cristobalite strikingly resemble that of  $v\text{-SiO}_2$ , unlike those of the two phases of quartz. The microscopic structures of  $\beta$ -cristobalite, HP-tridymite and  $v\text{-SiO}_2$  are similar over the length scale  $10 \text{ \AA}$ , indicating the internal flexibility of the cristobalite and tridymite structures. In these crystalline phases the disorder is dynamic

and driven by the need to avoid local configurations with linear Si–O–Si bonds, whereas the disorder in v-SiO<sub>2</sub> is static over conventional time-scales. See figure 8. The low temperature  $\alpha$ -phase does not have the same flexibility as the high-temperature crystalline phases. Thus, it is reasonable to assume that v-SiO<sub>2</sub> shows similarities with the local structures of  $\beta$ -cristobalite and HP-tridymite structures in which the tetrahedra easily rotate to change the bond angle to a more favourable value (Dove *et al* 1997, Keen and Dove 1999, Tucker *et al* 2001). The structural data on silica are given in table 1.

*Ab initio* molecular dynamics (MD) calculations have demonstrated that the network of v-SiO<sub>2</sub> consists of 6-membered rings together with 3-, 4-, 5-, and 7-membered rings (Sarnthein *et al* 1995, Pasquarello and Car 1998, Pasquarello *et al* 1998), where closed paths containing  $n$ -Si–O segments are referred to as  $n$ -membered rings. Though 6-membered rings dominate, the fraction of 5- and 7-membered rings are each about 10%, depending on the cooling rate of the system (see figure 6). Such evidence was obtained from the analysis of diffraction experiments in terms of high-energy x-ray scattering in addition to neutron scattering (Suzuya *et al* 2000, Kohara and Suzuya 2001). The existence of 3- and 4-membered rings are verified by RS experiments through the observation of D<sub>1</sub> and D<sub>2</sub> defect lines (see, e.g. Galeener and Geissberger 1983).

Embedded 5- and 7-membered rings may play a role in yielding ‘low-pressure’ bond-parts and ‘high-pressure’ bond-parts in v-SiO<sub>2</sub>. This situation is schematically illustrated in figure 7, which shows a pair-wise creation of 5- and 7-membered rings due to the bond-switching mechanism. It is important to note that Sokolov *et al* (1993) have estimated that the number density of modes contributing to the Boson peak is of the order of 10% for many types of glasses. This estimated number density is of the same order as that of mismatched 5- or 7-membered rings in v-SiO<sub>2</sub>.

**Table 1.** Structural data for the ambient pressure phases of silica.

	$\alpha$ -quartz	$\alpha$ -cristobalite	$\beta$ -cristobalite	v-SiO <sub>2</sub>	d-SiO <sub>2</sub>
$T$ (°C)	20	200	300	20	20
$\rho$ (g cm <sup>-3</sup> )	2.65	2.33	2.21	2.20	2.63
Si–Si (Å)	3.06	3.08	3.11	3.12	3.04 ± 0.11
Si–O (Å)	1.609	1.606	1.606	1.617	1.61
O–O (Å)	2.632	2.623	2.623	2.626	2.63
O–Si–O (°)	109.8	109.5	109.5	108.6	109.7
Si–O–Si (°)	144	147	151	145 ± 25	142 ± 25

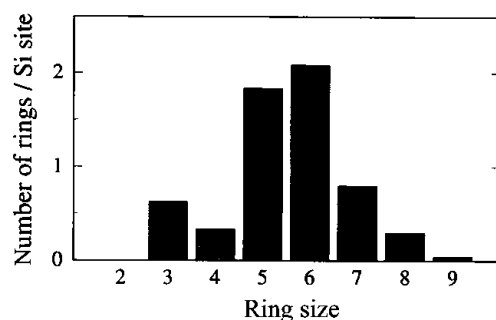


**Figure 6.** Ring statistics of v-SiO<sub>2</sub>. After Pasquarello and Car (1998).

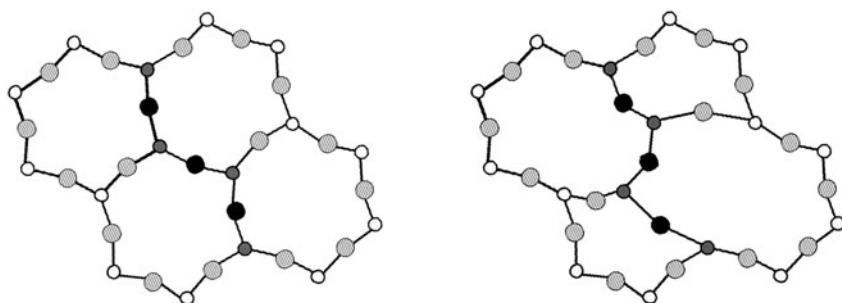


**Figure 7.** Schematic illustration of topological bond switch from 6-membered rings to 5- and 7-membered rings.

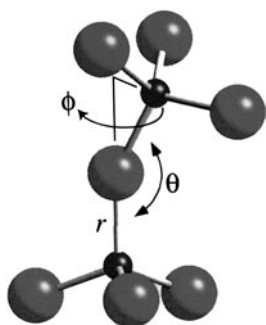


**Figure 8.** Schematic diagram representing buckled  $\text{SiO}_4$  tetrahedra at oxygen site.

It is suggestive to consider *oxygen defects* in Si crystals. As-grown Si crystals contain oxygen as interstitial bridging Si atoms, being situated in a slightly off-axis position between two nearest-neighbor Si atoms in the [111] direction, since the equilibrium spacing between Si atoms is smaller than the Si–Si bond length of the Si–O–Si segment. This leads to distortion at the oxygen sites, which we call *buckled* sites (see also figure 8). The triangle consisting of the Si–O–Si segment provides new degrees of freedom for vibrations or rotations perpendicular to the Si–O–Si plane (Yamada-Kaneda *et al* 1993). There is experimental evidence from infrared absorption experiments that reveal low-lying states due to oxygen impurities with eigenfrequencies at 29, 38, 43, and 49  $\text{cm}^{-1}$  (Bosworth *et al* 1970). The sequence of these low-lying energy levels has also been confirmed by phonon spectroscopic technique (Lassmann 1996). It should be noted that the observed frequency range 29–49  $\text{cm}^{-1}$  is identical with that for the Boson peak in  $\nu\text{-SiO}_2$ .

## 2.2. Effect of pressure on local structures

Irreversible densification of  $\nu\text{-SiO}_2$  occurs around 10 GPa (Bridgman 1949, Arndt 1969, 1983). The structure factor  $S(Q)$  observed for normal and densified amorphous silica ( $d\text{-SiO}_2$ ) indicates that the change of the shape of the  $\text{SiO}_4$  tetrahedron with short-range-order is very small, but there is a substantial change in the FSDP (Sinclair *et al* 1980, Moss and Price 1985, Wright *et al* 1985, Chervinka 1987, Fowler and Elliott 1987, Meade *et al* 1992), indicating a large modification in the MRO associated with the FSDP, as well as a significant reduction in

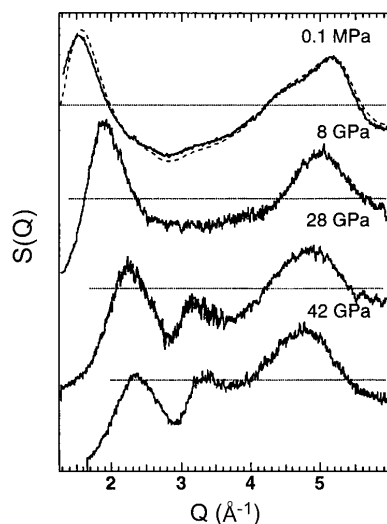


**Figure 9.** X-ray structure factor  $S(Q)$  of v-SiO<sub>2</sub> in the range of pressure 0.1 MPa to 42 GPa. Dashed lines are the data at ambient pressure. After Inamura *et al* (1998).

the width of the Si–O–Si angle distribution (Hemley *et al* 1986, Susman *et al* 1991). Figure 9 shows the density dependence of the total radial pair correlation function, in which the FSDP for normal v-SiO<sub>2</sub> clearly blue-shifts on densification (Inamura *et al* 1998). The pressure-induced changes in the FSDP are mainly due to the reduction in distances between Si atoms, related to the decrease in the Si–O–Si bond angles (see figure 5).

Mukherjee *et al* (2001) reported the direct verification of a first-order phase transition in amorphous silica from the low-density amorphous (LDA) to the high-density amorphous (HDA) phase of silica glass with an apparent discontinuous volume change of about 20% at 3.6 GPa and 680°C. Lacks (1998, 2000) predicted in terms of MD simulations that a kinetically hindered first-order amorphous-to-amorphous transition occurs in silica glass, suggesting that LDA–HDA is apparently a *first-order* phase transition with a discontinuous volume change of about 20% in the pressure range 3–5 GPa. Note that the difference in mass density between v-SiO<sub>2</sub> ( $\rho = 2.20 \text{ g cm}^{-3}$ ) and crystalline  $\beta$ -cristobalite ( $\rho = 2.21 \text{ g cm}^{-3}$ ) is only about 4%, whereas it is about 20% in the case of  $\alpha$ -quartz ( $\rho = 2.65 \text{ g cm}^{-3}$ ) similar to the HDA phase of silica glass (d-SiO<sub>2</sub>) ( $\rho = 2.63 \text{ g cm}^{-3}$ ). See table 1.

Hemley *et al* (1986) performed a high pressure Raman spectroscopic study for v-SiO<sub>2</sub> at room temperature. Figure 10 shows the Raman spectra of v-SiO<sub>2</sub> as a function of pressure (Hemley *et al* 1986). They revealed a gradual irreversible change in the Raman spectrum between 80 and 30 GPa in addition to a broadening of the Raman band and a loss of intensity above 30 GPa. There are also other types of experimental evidence (Grimsditch 1984, Polian and Grimsditch 1990) pointing to the existence of a gradual LDA to HDA phase transition in v-SiO<sub>2</sub> at pressures of 10–25 GPa, as well as in the case of amorphous ice (Mishima *et al* 1985). Stone *et al* (2001) investigated the neutron diffraction profile for pressure-compacted vitreous GeO<sub>2</sub> up to 6 GPa in order to examine their medium range structure. They found a strong dependence on pressure of the FSDP. The profile shown in figure 11 for d-GeO<sub>2</sub> at 1 atm shows the FSDP at  $Q_1 = 1.6 \text{ \AA}^{-1}$ . They suggested that changes in the first Ge–Ge peak with increasing density indicate a progressive reduction of the mean Ge–O–Ge bond angle.

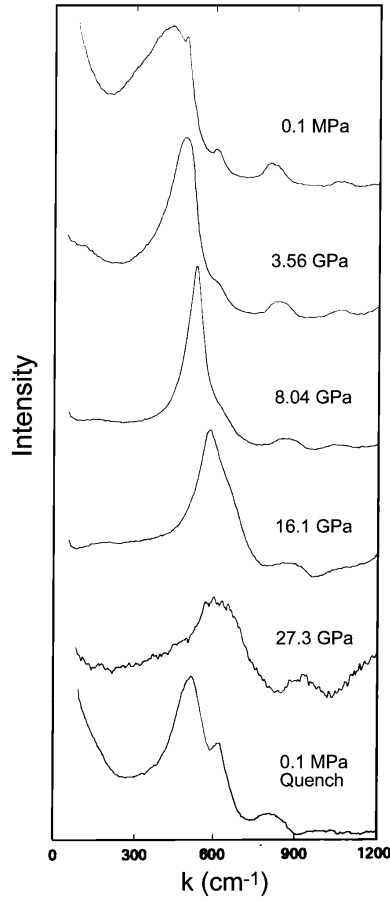


Figure 10. Raman spectra of v-SiO<sub>2</sub> as a function of pressure. After Hemley *et al* (1986).

### 3. Anomalous behaviours of v-SiO<sub>2</sub> at THz frequency range

#### 3.1. Excess densities of states

Flubacher *et al* (1959) was the first to find the excess specific heat for v-SiO<sub>2</sub> in the temperature range 2.2–19 K, which he ascribed to be of the same origin as that observed by RS at 30–120 cm<sup>-1</sup> by Krishnan (1953). The relation between the specific heat  $C(T)$  and the phonon DOS  $D(\omega)$  is expressed by the formula, using the definition of the inverse temperature  $\beta = 1/k_B T$ ,

$$C(T) = -\frac{1}{k_B T^2} \frac{\partial}{\partial \beta} \left[ \int_0^\infty n(\beta \hbar \omega) \hbar \omega D(\omega) d\omega \right], \quad (1)$$

where  $n(\beta \hbar \omega)$  is the BE distribution function. The DOS from the Debye theory is given by

$$D(\omega) = \frac{6\pi \omega^2}{\omega_D^3}, \quad (2)$$

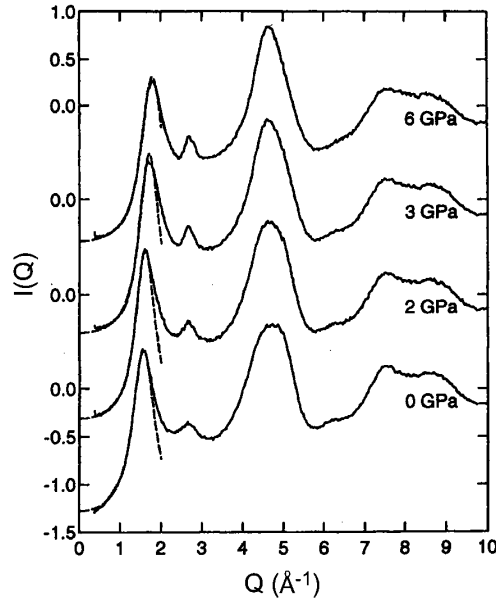


**Figure 11.** Neutron diffraction patterns for d-GeO<sub>2</sub>, together with Lorentzian fit (---) to the FSDP. After Stone *et al* (2001).

where the Debye frequency  $\omega_D$  is related to the velocities of transverse and longitudinal sound by

$$\omega_D^3 = \frac{9N}{32\pi^4 V} \left( \frac{2}{v_t^3} + \frac{1}{v_l^3} \right)^{-1}. \quad (3)$$

Here  $N$  is the number of atoms in the volume  $V$ . The experimental values of velocities for v-SiO<sub>2</sub> are  $v_t = 3.767 \times 10^5 \text{ cm s}^{-1}$  and  $v_l = 5.970 \times 10^5 \text{ cm s}^{-1}$ , respectively, which gives a Debye frequency  $\nu_D$  of 10.40 THz. Using the above relations, one has the Debye law,

$$C(T) = \frac{12\pi^4 N k_B}{5} \left( \frac{T}{\Theta_D} \right)^3, \quad (4)$$

with the Debye temperature  $\Theta_D = \hbar\omega_D/k_B = 500 \text{ K}$  for v-SiO<sub>2</sub>. One can obtain the DOS  $D(\omega)$  by inverting equation (1) from the data of  $C(T)$ . There is an ambiguity when obtaining  $D(\omega)$  from experimental data of  $C(T)$  by the procedure of the inversion transformation. However, this type of thermal measurement is not affected by the mode-selection rule on excited modes as in the case of optical spectroscopy measurements, in which case active modes are different for infrared scattering, RS, and hyper-Raman scattering (HRS). The hump in the temperature dependence of  $C$  is realized by plotting as  $C/T^3$  against  $T$  in the temperature range 10–30 K (Pohl 1981, von Löneysen *et al* 1985, Buchenau *et al* 1986). Sokolov *et al* (1997) analysed the excess specific heats of various glasses focusing on the concept of fragility (Angel 1995). They showed a strong dependence on fragility of the specific heats in the range in which the excess vibrational contribution is present. Typical data for the ratio of specific heats  $C$  for both v-SiO<sub>2</sub> and d-SiO<sub>2</sub> are shown in figure 12 (Inamura *et al* 1999), in which the data are compared with the predictions of the Debye theory.

The excess DOS of v-SiO<sub>2</sub> observed as a hump in the specific heat has been confirmed by RS (Winterling 1975), INS (Buchenau *et al* 1984, 1986, 1988) and infrared absorption

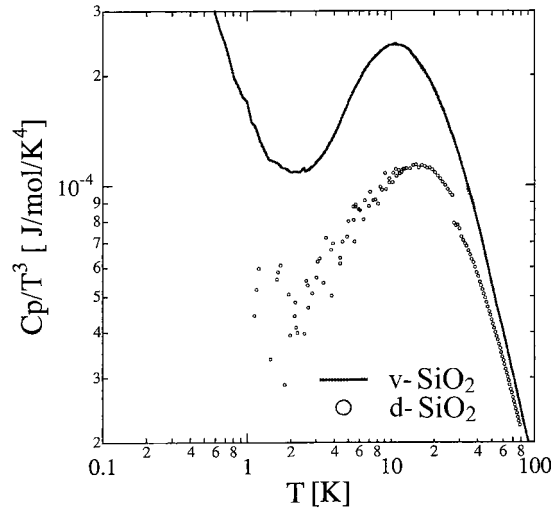


**Figure 12.** Specific heat  $C_P(T)$  of v-SiO<sub>2</sub> (—) and d-SiO<sub>2</sub> (○) plotted as  $C_P(T)/T^3$  against  $T$ . After Inamura *et al* (1999).

(Galeener *et al* 1983, Ohsaka and Oshikawa 1998, Ohsaka *et al* 1999), in addition to recent hyper-Raman experiments (Yamaguchi and Yagi 1999b, Helen *et al* 2000). The relation between the DOS and the RS intensity can be expressed as

$$I(\omega) = \frac{(n+1)}{\omega} D(\omega) C(\omega), \quad (5)$$

where  $D(\omega)$  is the DOS and  $C(\omega)$  is the Raman-coupling coefficient. Let us assume that the DOS  $D(\omega)$  has a broad and almost constant spectral distribution at around the Boson peak energy. Since the Bose factor  $(n+1)$  is proportional to  $T/\omega$  at temperatures larger than the Boson peak energy, the Raman intensity  $I(\omega)$  should have the tail proportional to  $1/\omega^{2-\alpha}$  provided that the Raman coupling coefficient  $C(\omega)$  is proportional to  $\omega^\alpha$  ( $\alpha = 0-2$ ). Note that the frequency dependence  $I(\omega) \propto 1/\omega$  for the case of  $\alpha = 1$  is the same with that of the *Bose distribution function*  $n(\beta\hbar\omega)$  at relevant temperatures. Malinovsky and Sokolov (1990) have pointed out that the Boson peak spectra obtained by RS experiments take the universal shape as mentioned above. In contrast, the shape of the second broad peak observed in the RS at around  $430 \text{ cm}^{-1}$  for v-SiO<sub>2</sub> is different from that of the Boson peak. The intensity continuously increases with frequency above the Boson peak. The shape of the second broad peak reflects the difference of the  $\omega$ -dependence of  $C(\omega)$  and  $D(\omega)$  for relevant modes above the Boson peak.

Helen *et al* (2000) and Yamaguchi and Yagi (1999b) have performed HRS experiments to investigate the modes relevant to the Boson peak in v-SiO<sub>2</sub>. Helen *et al* (2000) discovered that the Boson peak obtained from HRS is strong compared with those obtained from RS and infrared absorption. See figure 13. The modes leading to the peak in HRS are essentially silent both in infrared absorption and in RS. There is only one type of vibrational mode active in HRS that is forbidden in infrared absorption and RS (Cyvin *et al* 1965). This is the F<sub>1</sub> mode having the symmetry of the three infinitesimal rotation operators. This suggests that the Boson peak obtained by HRS is principally due to the mode involving rotational motion of SiO<sub>4</sub> tetrahedra. This mode had been suggested by Buchenau *et al* (1984, 1986) from the analysis of their INS data. The most striking result is the resemblance of the intensity  $I(\omega) \propto C(\omega)(n+1)D(\omega)/\omega$

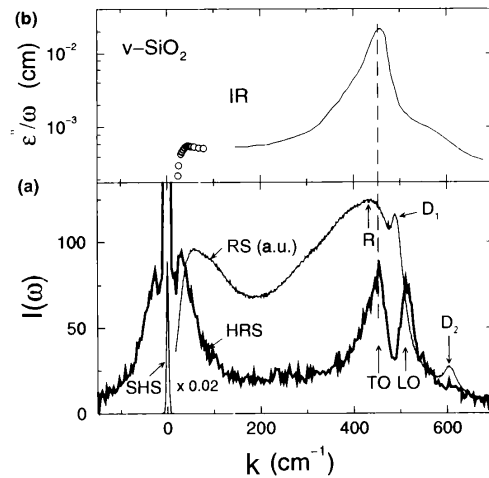


**Figure 13.** Light scattering and infrared spectra of  $\nu$ -SiO<sub>2</sub>. (a) Comparison of the intensities of spectra between HRS and RS at 90° in (V + H). The ordinate scale is for the HRS signal. (b) The imaginary part of the dielectric constant divided by  $\omega$  obtained from infrared reflectivity. After Helen *et al* (2000).

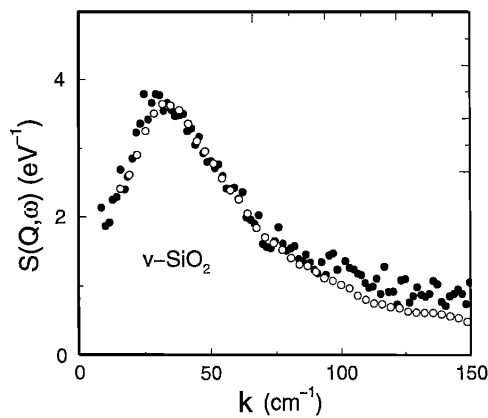


**Figure 14.**  $S(Q, \omega)$  from INS (○) and scaled hyper-Raman intensity  $I(\omega)$  (●). After Helen *et al* (2000).

obtained by HRS and the incoherent INS data  $S(\omega) \propto (n+1)D(\omega)/\omega$  (see figure 14), indicating the absence of a frequency dependence of the hyper-Raman coupling coefficient  $C(\omega) \propto \omega^0$ . From this evidence, Helen *et al* (2000) concluded that the main modes contributing to the Boson peak can be associated with those with a frequency-independent coupling coefficient  $C(\omega)$ . Their results lead to the following interpretation of the nature of the Boson peak: (i) The modes that produce the Boson peak in HRS are optic modes and their spectral distribution is almost identical with those measured by incoherent INS at the peak frequency of  $\nu \approx 1$  THz. (ii) Those vibrations are non-polar and the coupling coefficient  $C(\omega)$  is frequency-independent, as opposed to  $C(\omega) \propto \omega^2$  for acoustic-like modes. (iii) The DOS for the Boson peak is dominated by modes with a flat dispersion relation.

#### 4. Pressure dependence of the Boson peak

##### 4.1. RS under high pressure

RS experiments at high pressure reveal some important features of the THz dynamics of glasses. In order to interpret such features, Arai *et al* (1985) demonstrated the significant effect of pressure on the Boson peak in  $\alpha$ -As<sub>2</sub>S<sub>3</sub>. They found that the Boson peak centred at 20 cm<sup>-1</sup> is very sensitive to hydrostatic pressure. Hemley *et al* (1986) studied the pressure dependence of the Boson peak for  $\nu$ -SiO<sub>2</sub> by means of RS. They found a remarkable effect of the pressure on the Boson peak at 8 GPa in addition to a significant reduction in the width of the fluctuation of the Si–O–Si angle distribution. The RS spectrum of normal  $\nu$ -SiO<sub>2</sub> shows the profile given in figure 1. One sees that an entirely different pattern evolves on compression, as well as a marked shift of the Boson peak with pressure (Hemley *et al* 1997) (see figure 15). It should be emphasized that there is a collapse of the scattering intensity of the secondary diffuse band at 430 cm<sup>-1</sup> at a pressure of 8 GPa (Hemley *et al* 1986).

Yamaguchi *et al* (1998) and Yamaguchi and Yagi (1999a) performed RS experiments under pressures up to 2.6 GPa on the two-dimensional (2d)-network glass,  $\alpha$ -GeS<sub>2</sub>. Hydrostatic pressure was applied to the sample with a diamond anvil cell, and was varied from ambient pressure to 2.6 GPa. Figure 16 shows typical scattering spectra in the vicinity of the Boson peak for  $\alpha$ -GeS<sub>2</sub> on varying the hydrostatic pressure. Two apparent peaks are observed in this frequency region, namely, the Boson peak indicated by arrows and the secondary peaks in the vicinity of 100–150 cm<sup>-1</sup>. The maximum frequency of the Boson peak shifts to higher frequencies with increasing pressure. In particular, the Boson peak becomes broader and the relative intensity of the Boson peak compared with the secondary peak decreases with pressure. All these effects were reversible within their pressure range. The reversibility of these changes indicates that the pressure effects on the Boson peak reflect the strong anharmonicity of the corresponding *local* potentials near their minima, in addition to the strong anharmonic coupling between the modes relevant to the Boson peak and the long-wavelength acoustic modes corresponding to pressure waves.

RS spectra by Yamaguchi and Yagi (1999a) taken under conditions of hydrostatic pressure up to 2.6 GPa for  $\alpha$ -GeS<sub>2</sub> have generated values for the third-order vibrational anharmonicity associated with the Boson peak modes some *twenty* times that associated solely with the long-wavelength acoustic modes. This provides evidence for the strong anharmonicity of the

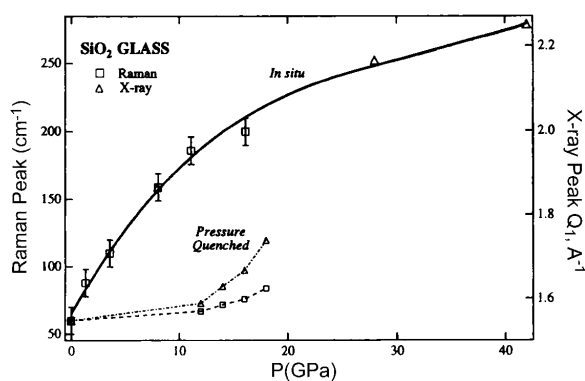


**Figure 15.** Pressure dependence of the maximum of the Boson peak and the FSDP  $Q_1$  for  $\nu$ -SiO<sub>2</sub>. After Hemley *et al* (1997).

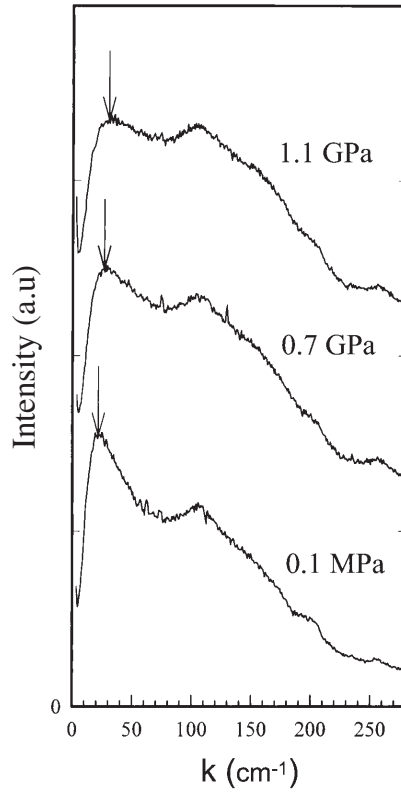


**Figure 16.** RS spectra of a-GeS<sub>2</sub> in the low-frequency region at various hydrostatic pressures. After Yamaguchi and Yagi (1999a,b).

potentials associated with the Boson peak spectrum. They have estimated from the shift of the Boson peak the anharmonic coefficient arising from the coupling between the modes relevant to the Boson peak (S) and longitudinal acoustic (P) modes to be ,

$$C_{SSP} \approx -5.4 \times 10^{13} \text{ dynes cm}^{-2}, \quad (6)$$

while the third-order elastic coupling for longitudinal acoustic modes alone is, from Brillouin data,

$$C_{PPP} \approx -2.2 \times 10^{12} \text{ dynes cm}^{-2}. \quad (7)$$

These results clearly demonstrate the much larger anharmonicity associated with the Boson peak as compared to the acoustic vibrations, by nearly *a factor of 25*. Also, the observed Raman *intensity* of the Boson peak diminishes rapidly with increasing pressure, as compared to the higher vibrational bands for which there is only a very small intensity change with increasing pressure. Because the Raman intensity is proportional to the square of the relative atomic displacement, this means that the relative atomic motions associated with the Boson peak are much more strongly reduced with increasing pressure than for the relative motions associated with the higher energy vibrational bands.

#### 4.2. Boson peak of d-SiO<sub>2</sub>

Inamura *et al* (1998, 1999, 2000) demonstrated the excess DOS of d-SiO<sub>2</sub> in INS experiments. They prepared samples of both normal v-SiO<sub>2</sub> and d-SiO<sub>2</sub> with densities 2.20 and 2.63 g cm<sup>-3</sup>.

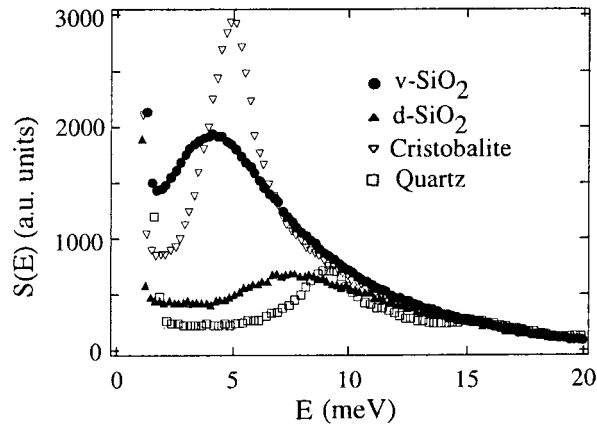


**Figure 17.** Integrated  $S(Q, \omega)$  in  $Q$ -range from 1 to  $7 \text{ \AA}^{-1}$  for v-SiO<sub>2</sub>, d-SiO<sub>2</sub>, polycrystalline  $\alpha$ -cristobalite, and polycrystalline  $\alpha$ -quartz as a function of the energy transfer. After Inamura *et al* (1998) and Nakamura *et al* (2002).

Figure 17 shows their results for the integrated dynamic structure factor  $S(Q, \omega)$  in  $Q$ -range from 1 to  $7 \text{ \AA}^{-1}$  for both samples in addition to  $\alpha$ -cristobalite and  $\alpha$ -quartz. The Boson peaks of both samples appear at 4 meV for normal SiO<sub>2</sub> and 7.5 meV for d-SiO<sub>2</sub>, respectively. (Note that 1 meV = 0.242 THz.) In particular, the peak intensity for v-SiO<sub>2</sub> and d-SiO<sub>2</sub> drastically decreases in the THz frequency region, where there is no observable difference between normal and densified v-SiO<sub>2</sub> above 12 meV in the DOS. This indicates that the Boson peak in normal v-SiO<sub>2</sub> is remarkably suppressed due to densification, and does not show a simple shift of the spectra to a higher energy region. The same tendency was observed for d-GeO<sub>2</sub> by Suzuya *et al* (2001). These works suggest that *the Boson peak is very much affected by densification*.

Mukherjee *et al* (2001) have carried out RS experiments for d-SiO<sub>2</sub>. They found that the diffuse spectrum observed for normal v-SiO<sub>2</sub> at  $430 \text{ cm}^{-1}$  disappears in d-SiO<sub>2</sub> apart from a small hump at about  $500 \text{ cm}^{-1}$ . It is natural to interpret the suppression of the DOS of the Boson peak due to densification as being related to the shrinkage of open structures of, say, 6- and 7-membered rings in normal v-SiO<sub>2</sub> (see figure 7). This view is consistent with the structural investigations of pressurized d-SiO<sub>2</sub> with Raman spectroscopy (Hemley *et al* 1986) and NMR (Devine *et al* 1987). Sugai and Onodera (1996) performed RS experiments for d-GeO<sub>2</sub> and obtained similar tendencies to those for d-SiO<sub>2</sub> mentioned above. We note that Novikov and Sokolov (1991) and Sokolov *et al* (1992) had suggested the existence of a correlation between the Boson peak and the FSDP.

## 5. Phonon transport in v-SiO<sub>2</sub>: the existence of the crossover frequency $\nu_0$ to phonon localization

### 5.1. Thermal conductivities at the plateau temperature region

Thermal conductivity measurements provide valuable information on localization and/or delocalization of excited phonons in glasses. The thermal conductivity  $\kappa(T)$  is expressed by the formula for an isotropic material,

$$\kappa(T) = \frac{1}{3} \sum_{j=1}^3 \int_0^{\omega_D} C_j(\omega) v_j(\omega) l_j(\omega) d\omega, \quad (8)$$

where the sum is over the polarization  $j$  of *propagating* phonons,  $v_j$  and  $l_j$  are the phonon group velocity and mean-free-path of the polarization  $j$ , and  $C_j(\omega)$  is its contribution to the phonon specific heat having angular frequency  $\omega$ , respectively. The typical temperature dependence of  $\kappa(T)$  for  $\alpha$ -quartz is shown by the upper curve in figure 2. In the temperature region below around 10 K, the phonon mean-free-path  $l_j(\omega)$  becomes mostly much longer than the sample size. Combined with the constant velocities of acoustic phonons,  $\kappa$  for crystals should have the same temperature dependence as that of the specific heat proportional to  $T^3$  as shown in figure 2. Above about 10 K, phonons are scattered by intrinsic processes such as phonon–phonon and Umklapp processes (Peierls 1929), leading to a decrease of  $\kappa(T)$  with increasing temperature  $T$ . Since thermal conductivities at low temperatures are dominated by long-wavelength propagating phonons, it is natural to consider that there is no difference between glasses and crystals in this temperature regime. This is because long-wavelength phonons excited below 10 K are insensitive to structure on microscopic length-scales smaller than the corresponding wavelength  $\lambda$ . However, the observed thermal conductivities for glasses behave quite differently from those of crystals, as shown in figure 2.

The qualitative frequency dependence of the phonon mean-free-path  $l_s(\omega)$  in glasses is shown in figure 18, as estimated from experimental data of  $\kappa(T)$  given in figure 2. If the frequency dependence of  $l_s(\omega)$  given in figure 18 is correct, this leads to the following interpretation of  $\kappa(T)$ : (i) at low temperatures below a few Kelvin, propagating acoustic phonons are scattered by the TLS, and one has the relation  $\kappa(T) \propto T^2$ , (ii) at higher temperatures (the plateau region), propagating acoustic phonons are exhausted at a crossover frequency  $\nu_0$ , leading to a  $\kappa(T) = \text{const.}$  (the Dulong–Petit limit), and (iii) at temperatures above the plateau an additional heat transfer channel opens. Thus, glasses behave as a low-pass filter indicating that the heat is carried only by low-frequency phonons  $\nu < \nu_0$ .

Zhu (1994) measured the thermal conductivity  $\kappa(T)$  of d-SiO<sub>2</sub> from 15 K to room temperature and found that  $\kappa(T)$  displays a plateau at temperatures up to 60 K, and that the magnitude of the plateau becomes higher than that of normal v-SiO<sub>2</sub>. This experiment indicates that the plateau is severely affected by the densification. These results can be interpreted as being due to the crossover frequency  $\nu_0$  of localization for acoustic phonons shifting to higher frequencies and the total number of propagating acoustic phonons contributing to heat transfer increasing with densification.

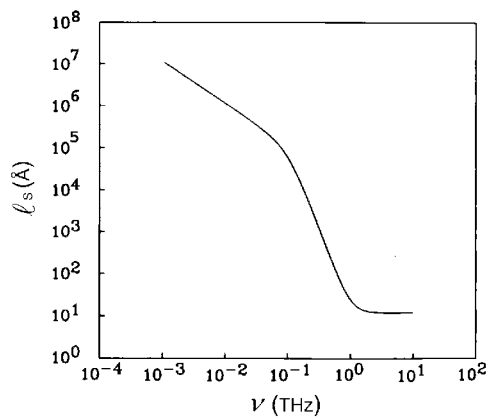


**Figure 18.** Estimated frequency dependence of the phonon mean-free-path  $l_s(\omega)$  from the analysis of  $\kappa(T)$  for v-SiO<sub>2</sub>. After Graebner *et al* (1986).

### 5.2. Kapitza thermal boundary conductance

Direct evidence that figure 18 can be qualitatively correct is obtained from the measurements of the Kapitza thermal boundary conductance  $h_K$  for the interface between a glass (G) and a non-glassy solid (S), which presents the transmission coefficient  $t_{GS}(\theta_{q_j})$  for an incoming propagating phonon of wavevector  $\mathbf{q}_j$  with the polarization  $j$  incident at angle  $\theta_{q_j}$  across the interface. How the transmission coefficient  $t_{GS}(\theta_{q_j})$  across the boundary is introduced in the conductance  $h_K$  is shown below according to a text by Nakayama (1989). When a propagating phonon with frequency  $\hbar\omega$  is incident from a glass (G) onto a non-glassy solid (S), an energy  $\hbar\omega t_{GS}(\theta_{q_j})$  is transmitted to the non-glassy solid. As a result, the heat flux  $\dot{Q}_{GS}$  from a glass (G) to a non-glassy solid (S) is defined by

$$\dot{Q}_{GS}(T) = \frac{1}{(2\pi)^3} \sum_{j=1}^3 \int_0^{q_D} n(\omega) v_j \cos \theta_{q_j} \hbar\omega t_{GS}(\theta_{q_j}) d^3 q_j, \quad (9)$$

where the angular integral  $\theta_{q_j}$  should be performed in a half space. At low temperatures the BE distribution function  $n(\beta\hbar\omega)$  becomes sharp and excited phonon frequencies  $\nu = \omega/\hbar$  are simply related to the temperature  $T$  by the formula  $\nu = 4.8 \times 2 \times 10^{10} T$  (Hz K<sup>-1</sup>)  $\approx 0.1 T$  (THz K<sup>-1</sup>). Assuming the Debye DOS for acoustic propagating phonons, the integral of equation (9) yields (Nakayama 1989), under the approximation of average phonon velocities,

$$\dot{Q}_{GS}(T) = \frac{\pi^2 \rho_G \bar{v}_G k_B^4 T^4}{10 \rho_S \bar{v}_S^3 \hbar^3} F_{GS}, \quad (10)$$

where  $\bar{v}_G$  and  $\bar{v}_S$  are the average phonon velocities in a glass (G) and a non-glassy solid (S), respectively. Also,  $\rho_G$  and  $\rho_S$  are the mass density of a glass and a solid, respectively. The factor  $F_{GS}$  is given by

$$F_{GS} = \frac{\rho_S}{2\rho_G} \left( \frac{\bar{v}_S}{\bar{v}_G} \right)^3 \int_0^1 t_{GS}(\theta) \cos \theta d(\cos \theta). \quad (11)$$

If the transmission coefficient  $t_{GS}(\theta)$  on average is not a function of frequency  $\omega$ , the heat flux  $\dot{Q}_{GS}$  will be proportional to  $T^4$  as seen from equation (10).

The temperature jump  $\Delta T$  between two materials arises because the probability  $t_{GS}(\theta)$  is less than unity. This limits the heat current out of the hotter medium, and so the interface acts as a thermal barrier across which a temperature difference can be sustained. The proportionality constant relating the temperature jump  $\Delta T$  to heat flux  $\dot{Q}$  between two materials is known as the Kapitza conductance  $h_K$ . Thus, one has

$$\dot{Q} = h_K \Delta T, \quad (12)$$

where the Kapitza conductance  $h_K$  is defined by

$$h_K = \frac{\partial \dot{Q}_{GS}(T)}{\partial T}, \quad (13)$$

while the Kapitza resistance  $R_K$  is defined by the relation  $R_K = 1/h_K$ . Defining the average transmission coefficient by

$$\bar{t}_{GS} = 2 \int_0^1 t_{GS}(\theta) \cos \theta d(\cos \theta), \quad (14)$$

the conductance  $h_K$  can be expressed as, from equations (10) and (14),

$$\frac{h_K}{T^3} = c \bar{t}_{GS}, \quad (15)$$

where  $c$  takes a constant value determined by material constants, and where the quotient  $h_K/T^3$  has no adjustable parameters. This treatment is known as the acoustic mismatch theory (Khalatnikov 1952). It should be noted that Jäckle (1983) theoretically investigated the thermal boundary resistance at the interface between a crystalline and a disordered solid with large scattering mismatch but negligible acoustic mismatch, and showed the former contribution is additive to the acoustic mismatch channel.

Measurements of the Kapitza conductance  $h_K = 1/R_K$  were made, though not for v-SiO<sub>2</sub>, by Matsumoto *et al* (1977) for the case of epoxy resin glass and copper, where the epoxy glass plays a role as an adhesive. The epoxy layer had a well-defined thickness but was very thin, of the order of several tens of micrometres. Thermometers were placed on the copper, in rod form, as close to the interface as possible, and the sum of the thermal boundary resistances of the copper–epoxy and epoxy–copper interfaces was measured. Copper has a very high thermal conductivity, making the temperature drops inside it unimportant, and the electrons thermalize the phonons so that the thermometers measure the appropriate temperature distributions. Moreover, the adhesion of the interface between the epoxy and the copper was apparently quite good and the results were reproducible.

From the data plotted in figure 19, one sees that there are two distinct temperature regions in which the physical properties of  $\bar{t}_{GS}$  are quite different in the two regimes  $T < 0.01$  K and  $T > 1$  K. There is a decrease by 3 orders of magnitude in the quantity  $\bar{t}_{GS}$  as the temperature is increased from 1 to 10 K. This behaviour apparently indicates that only low-frequency phonons can contribute to phonon transmission across the interface, suggesting that other high frequency phonons are *non-propagating* and *localized*. The onset of localization plays a key

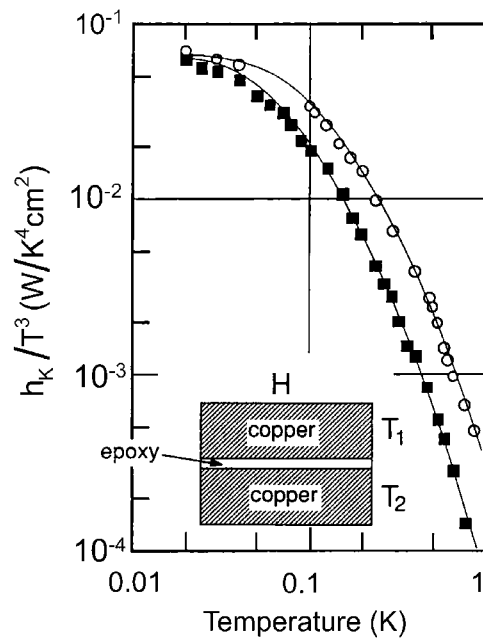


**Figure 19.** Measured transmission coefficients defined by equation (15) of copper–epoxy–copper sandwiches. Solid squares are for an epoxy layer of 80  $\mu\text{m}$  and open circles for an epoxy layer of 16  $\mu\text{m}$ . Schematic of the experimental geometry is shown in the inset. After Matsumoto *et al* (1977).

role for interpreting the plateau in the observed  $\kappa(T)$ . The question now arises as to the mechanisms responsible for phonon localization.

## 6. Inelastic neutron and x-ray scattering measurements

A variety of scattering experiments sensitive to the vibrational modes of  $v\text{-SiO}_2$  in the THz frequency range have been performed, among which INS and inelastic x-ray scattering (IXS) experiments are especially powerful for investigating the THz frequency dynamics. These two are complementary with their own advantages and limitations. It should be emphasized at first that the quantity obtained by these scattering experiments, say, the dynamical structure factor  $S(Q, \omega)$ , is the one projected onto plane-waves since it is defined through the spatial Fourier transformation. Thus, one should clarify the meaning of energy width of *localized vibrational modes* above the crossover frequency  $\nu_0$ . Obviously, exact eigenstates defined in energy have no energy width. It is only when one projects them onto plane-wave states that a lifetime is generated equally in frequency or wave vector space. When calculating an energy width for the localized modes, it should be understood to be that width which a plane-wave would experience, and  $Q$  loses its meaning as the wave vector.

### 6.1. INS for $v\text{-SiO}_2$

The energy of neutrons of the appropriate wavelength  $\lambda$  for structural and dynamic studies corresponds to thermal energies for temperatures from a few Kelvin to well above room temperature. Because of this wavelength–energy relation, neutron scattering is a powerful technique for the study of static and dynamic structure on the atomic scale (Lovesey 1984, Squires 1984, Bée 1988). The analysis and the interpretation of the data obtained by INS experiments for glasses are not simple compared with those of crystals because of the lack of long-range order of the atomic positions (Carpenter and Pelizzari 1975, Carpenter and Price 1985, Price and Carpenter 1987). Consequently, there is no complete destructive or constructive interference for scattered waves of neutrons, giving rise to Bragg peaks in the elastic scattering, and to momentum-conserving selection rules in the one-phonon inelastic scattering as in the case for crystals. In glasses, one cannot work around Bragg peaks as in crystals since coherent INS in the appropriate  $Q$ – $\omega$  space is limited by kinematical conditions due to the conservation of energy and wave-vector. In addition, caution is needed to extract the densities of states  $D(\omega)$  from the observed dynamical structure factor  $S(Q, \omega)$ , especially for the case of multicomponent systems such as  $v\text{-SiO}_2$ .

The dynamic structure factor  $S(Q, \omega)$  is proportional to the space-time Fourier transform of the density–density correlation function defined by  $G(|\mathbf{r} - \mathbf{r}'|, t) = \langle \rho(\mathbf{r}, t) \rho(\mathbf{r}', 0) \rangle$ , where  $\rho(\mathbf{r}, t)$  is the number density at time  $t$  and the angular brackets denote an equilibrium ensemble average. The atomic number density variations induced by atomic vibration with displacement  $\mathbf{u}_m(t)$  is defined as

$$\rho(\mathbf{r}, t) = \sum_m \delta(\mathbf{R}_m + \mathbf{u}_m(t) - \mathbf{r}), \quad (16)$$

where  $\mathbf{R}_m$  denotes the equilibrium position of nucleus  $m$ . The  $Q$ -component of the spatial Fourier transform becomes

$$\rho_Q(t) = \sum_m e^{-iQ \cdot \mathbf{r}_m(t)}, \quad (17)$$

where the definition is  $\mathbf{r}_m(t) = \mathbf{R}_m + \mathbf{u}_m(t)$ . The dynamical structure factor  $S(\mathbf{Q}, \omega)$  is proportional to the differential cross section for neutron scattering through the formula,

$$\frac{d^2\sigma}{d\Omega dE} = \frac{k_f}{k_i} \frac{\bar{\sigma}}{4\pi} e^{-\beta\hbar\omega/2} S(\mathbf{Q}, \omega), \quad (18)$$

where  $\hbar k_i$  and  $\hbar k_f$  are the strength of the initial and final momenta of the neutron,  $\hbar\mathbf{Q} = \hbar(\mathbf{k}_f - \mathbf{k}_i)$  and  $\hbar\omega = (\hbar^2/2m)(k_f^2 - k_i^2)$  are the changes of momentum and energy, respectively.  $\bar{\sigma}$  is an arbitrarily chosen microscopic scattering cross section. The dynamic structure factor  $S(\mathbf{Q}, \omega)$  is expressed by

$$S(\mathbf{Q}, \omega) = \frac{1}{2\pi\hbar N} \int_{-\infty}^{\infty} dt e^{-i\omega t} \sum_{m,n} \bar{b}_m \bar{b}_n \langle e^{i\mathbf{Q}\cdot\mathbf{r}_m(t)} e^{-i\mathbf{Q}\cdot\mathbf{r}_n(0)} \rangle, \quad (19)$$

where  $\bar{b}_m$  is the neutron scattering length of atom  $m$ , and  $N$  is its total number. The bar over  $b_m$  means spin and isotope averaging and the angular brackets indicate thermal averaging. It is convenient to express each term in equation (19) as a weighted sum for coherent scattering,

$$S(\mathbf{Q}, \omega) = \frac{4\pi}{N\bar{\sigma}} \sum_{m,n} \bar{b}_m \bar{b}_n S_{mn}(\mathbf{Q}, \omega), \quad (20)$$

where the sum is taken over all atoms  $m, n$  ( $m \neq n$ ) of the system. By expanding the atomic displacement  $\mathbf{u}_m(t)$  in terms of eigenmodes  $\lambda$ , one has

$$\mathbf{u}_m(t) = \sum_{\lambda} \left( \frac{\hbar}{2M_m\omega_{\lambda}} \right)^{1/2} \mathbf{e}_{\lambda} (\varphi_{\lambda}(\mathbf{R}_m) b_{\lambda}^+(t) + \text{h.c.}), \quad (21)$$

where h.c. means the Hermitian conjugate,  $\mathbf{e}_{\lambda}$  is the polarization vector of the  $\lambda$ -mode, and  $\varphi_{\lambda}(\mathbf{R}_m)$  the associated vibrational wavefunction. The  $b_{\lambda}^+$  ( $b_{\lambda}$ ) is the creation (annihilation) operator of the state  $\lambda$ . By expanding equation (17) in terms of small displacements  $\mathbf{u}_m(t)$ , one obtains for the first-order fluctuation

$$\Delta\rho_{\mathbf{Q}}(t) = \sum_{\lambda} \Delta\rho_{\lambda}(\mathbf{Q}, t) + O(u^2), \quad (22)$$

where the first term is defined as

$$\Delta\rho_{\lambda}(\mathbf{Q}, t) = e^{-i\omega_{\lambda}t} \Delta\rho_{\lambda}(\mathbf{Q}), \quad (23)$$

which gives the process contributing to creation or annihilation of *one phonon*, and  $\Delta\rho_{\lambda}(\mathbf{Q})$  is defined by

$$\Delta\rho_{\lambda}(\mathbf{Q}) = -i\hbar \sum_{\lambda,m} \frac{\mathbf{Q}\cdot\mathbf{e}_{\lambda}}{(2M_m\omega_{\lambda})^{1/2}} e^{-i\mathbf{Q}\cdot\mathbf{R}_m} (\varphi_{\lambda}(\mathbf{R}_m) b_{\lambda}^+(t) + \text{h.c.}). \quad (24)$$

$O(u^2)$  represents the contribution from the two-phonon process.

By substituting equation (24) into equation (19), one has the coherent inelastic term for the dynamic structure factor as

$$S(\mathbf{Q}, \omega) = \frac{n(\beta\omega) + 1}{N\bar{\sigma}} \sum_{\lambda} 4\pi\delta(\omega - \omega_{\lambda}) \left\langle \left| \sum_m \bar{b}_m \frac{\mathbf{Q}\cdot\mathbf{e}_{\lambda}\varphi_{\lambda}(\mathbf{R}_m)}{(2M_m\omega_{\lambda})^{1/2}} e^{-i\mathbf{Q}\cdot\mathbf{R}_m} \right|^2 \right\rangle, \quad (25)$$

where  $n(\beta\omega)$  is the Bose-Einstein (BE) distribution function and the brackets  $\langle \dots \rangle$  mean the orientational average of the direction of the vector  $\mathbf{Q}$ . We see from equation (25) that  $S(\mathbf{Q}, \omega)$  becomes a *flattened* dispersion independent of  $\mathbf{Q}$ , if one takes a strongly localized (sl) form

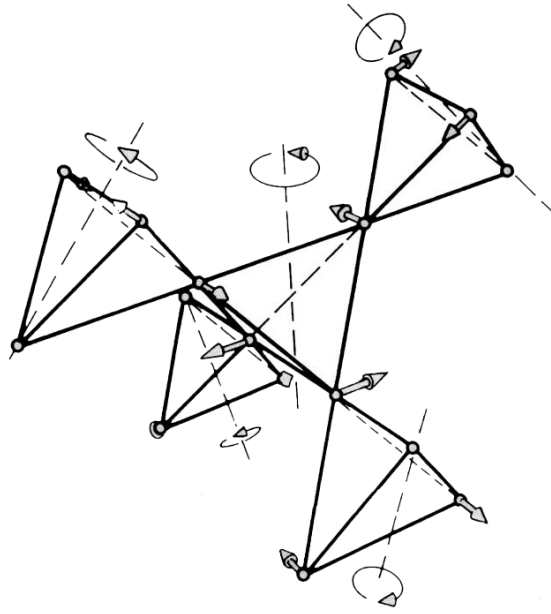


**Figure 20.** Coupled rotation of  $\text{SiO}_4$  tetrahedra as deduced from INS experiments. After Buchenau *et al* (1986).

for  $\varphi_\lambda(\mathbf{R}_m)$ . The isotropic nature of glasses should be taken into account on performing orientational averages, and the differential cross section becomes a function of only the magnitude of the momentum transfer  $\hbar Q = \hbar|\mathbf{Q}|$ . Carpenter and Pelizzari (1975) analytically demonstrated that the orientation-averaged  $S(Q, \omega)$  for one-phonon scattering process should appear with pseudo-periodicity in  $Q$ -space as a form of the zeroth and second-order spherical Bessel functions if the system possesses definite short-range order, as for example, within  $\text{SiO}_4$  tetrahedra in  $v\text{-SiO}_2$  (see figure 20).

Arai *et al* (1999a,b) performed INS experiments to investigate in detail the THz frequency dynamics of  $v\text{-SiO}_2$  over a wide range of energy ( $\hbar\omega$ ) and momentum ( $Q$ ) space using the MARI spectrometer in the ISIS facility at the Rutherford Appleton Laboratory. MARI is a chopper spectroscopy covering a wide range of  $Q$ - $\omega$  space, and gives 2d data of  $S(Q, \omega)$  in one measurement. Figure 21 gives  $S(Q, \omega)E/Q$ , together with  $S(Q)$ , in order to make the observed intensity more sensitive to small intensity variations over a wide range of the  $Q$ - $\omega$  space, since  $S(Q, \omega)$  is proportional to  $Q^2/E$  as shown in equation (25). Hence, this treatment enhances the intensity in high- $E$  regions and suppresses it in high- $Q$  regions. The observed data obtained at the incident energy  $\hbar\omega_i = 100$  meV with an energy resolution of 0.7 meV show clearly the pseudo-periodicity along the  $Q$ -axis as suggested by Carpenter and Pellizzari (1975) and by Carpenter and Price (1985). There clearly exist phonon pseudo-dispersion curves extending up to 50 meV with slightly variable periodicity reflecting the periodicity of  $S(Q)$ .

The  $Q$ -dependence of the Boson peak energy is depicted in figure 22. It is evident from figure 22 that the Boson peak does not show any dispersive behaviour in the  $Q$  range from 0.5 to  $6 \text{ \AA}^{-1}$  nor any of the pseudo-periodicity of the spherical Bessel function of Carpenter and Pellizzari (1975). Note that the flattened dispersion is a *necessary* condition for the existence of sl modes in the sense of its plane-wave Fourier transform. Another interesting feature noticed by Arai *et al* (1999a,b) is the existence of dispersive modes with the relation  $\omega \propto Q$  above

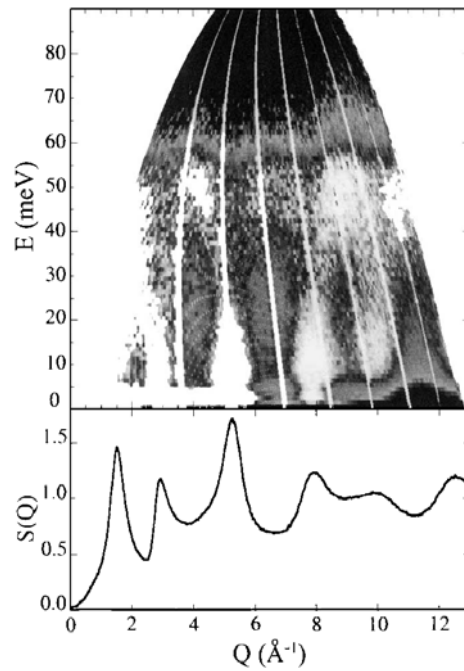


**Figure 21.** Contour map of  $S(Q, \omega)E/Q$  of v-SiO<sub>2</sub>. After Arai *et al* (1999a).

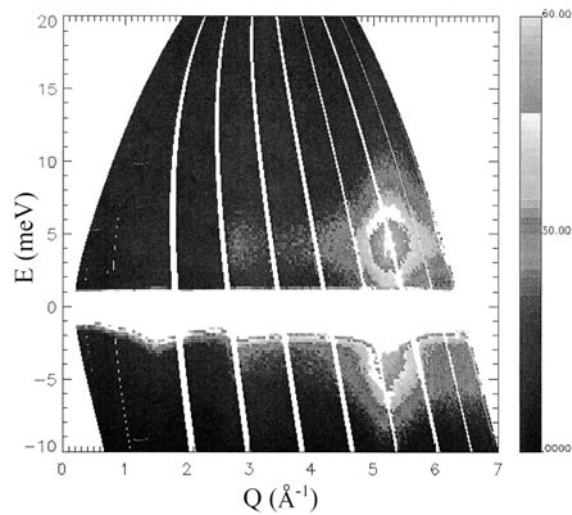


**Figure 22.**  $S(Q, \omega)E/Q$  at the Boson peak energy region. After Arai *et al* (1999b).

the Boson peak energy. The vibrations can be attributed to collective vibrations consisting of modes reflecting connected tetrahedra.

Nakamura *et al* (2001) performed INS experiments for v-SiO<sub>2</sub>,  $\alpha$ -cristobalite and  $\alpha$ -quartz. They found clear dispersive behaviour extending to 55 meV (1 THz = 4.14 meV) for these samples (see figure 23). In particular, the  $Q$ - $E$  relations show a similar behaviour for v-SiO<sub>2</sub>

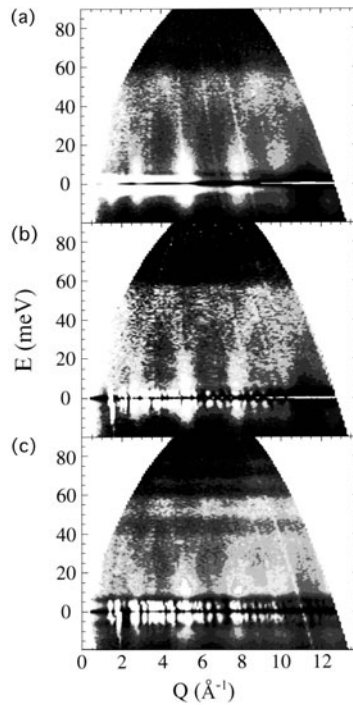


**Figure 23.**  $S(Q, \omega)E/Q$  contour maps of (a)  $v\text{-SiO}_2$ , (b)  $\alpha\text{-cristobalite}$ , and (c)  $\alpha\text{-quartz}$ . After Inamura *et al* (2001).

and for  $\alpha\text{-cristobalite}$  in the range of  $E \geq 7$  meV, because of the similarity in local structure of these samples. The behaviour of the pseudo-dispersion relation observed in  $v\text{-SiO}_2$  suggests that Umklapp processes also exist (Buchenau *et al* 1999, Scopigno *et al* 2001) as well as in the case of glassy Se (Foret *et al* 1998). The flattening of the dispersion relation centred at around 5 meV (Boson peak) shown in figure 24 is remarkable.  $S(Q, \omega)$  for  $\alpha\text{-cristobalite}$  has a narrower band at around 5 meV and a number of Bragg peaks can be observed.

Harris *et al* (1999) obtained by means of coherent INS,  $S(Q, \omega)$  for  $v\text{-SiO}_2$  and  $\alpha\text{-cristobalite}$  over a wide range of wavevectors ( $Q = 0.4\text{--}7.3 \text{ \AA}^{-1}$ ) in the Boson peak energy range. They suggested, by comparison with scattering data and from the similarity in the short-range order of both materials, that the Boson peak in  $v\text{-SiO}_2$  arises from the modes possessing a transverse nature (torsional motion of tetrahedra). A similar idea had been originally suggested by Leadbetter (1969).

## 6.2. IXS for $v\text{-SiO}_2$

IXS is a complementary method to INS for investigating acoustic modes in glasses at small momentum transfers  $Q$ . This method is based on a scattering process of a beam of photons, with energy  $\hbar\omega_i$ , momentum  $\hbar\mathbf{k}_i$ , and polarization  $\epsilon_i$ , impinging on a sample. Photons scattered with a specific energy  $\hbar\omega_f$ , momentum  $\hbar\mathbf{k}_f$ , and polarization  $\epsilon_f$  are detected, giving information on the spectrum of the excitations of energy  $\hbar\omega = \hbar\omega_i - \hbar\omega_f$  and momentum  $\hbar\mathbf{Q} = \hbar\mathbf{k}_i - \hbar\mathbf{k}_f$ . The IXS technique has become possible through the use of the high x-ray spectral flux density available from synchrotron radiation sources. An energy resolution of  $1.54 \pm 0.2$  meV is obtained by energy analysis of typically 20 keV x-rays at the European Synchrotron Radiation

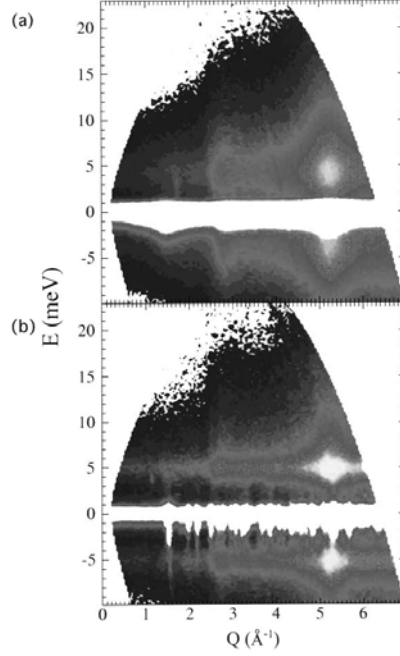


**Figure 24.**  $S(Q, \omega)$  contour maps at around 5 meV of (a) v-SiO<sub>2</sub> and (b)  $\alpha$ -cristobalite. After Nakamura *et al* (2001).

Facility in Grenoble. An incident wavelength  $\lambda_i = 0.5700 \text{ \AA}^{-1}$  is used, and other instrumental parameters are a Q-resolution of  $\pm 0.02 \text{ \AA}^{-1}$  and a photon flux of about  $2 \times 10^8 \text{ photons s}^{-1}$  (Ruocco and Sette 2001).

The differential cross section for incident photons with momentum  $\hbar \mathbf{k}_i$  is given by first-order perturbation theory as

$$\frac{d^2\sigma}{d\Omega dE} = r_0^2 (\boldsymbol{\epsilon}_i \cdot \boldsymbol{\epsilon}_f)^2 \frac{k_f}{\hbar k_i} \sum_f \left| \left\langle f, \mathbf{k}_f \left| \sum_m f_m(\mathbf{Q}) e^{i\mathbf{Q} \cdot \mathbf{R}_m} \right| i, \mathbf{k}_i \right\rangle \right|^2 \delta(\omega - \omega_f - \omega_i), \quad (26)$$

where  $r_0 = e^2/m_e c^2$  is the classical electron radius, and  $|i, \mathbf{k}_i\rangle$  and  $|f, \mathbf{k}_f\rangle$  are the ket representations of the initial and final state of the system, respectively. The  $f_m(\mathbf{Q})$  is the form factor of the atom  $m$  whose centre of mass position is  $\mathbf{R}_m$ . The form factor is the spatial Fourier transform of the electron-density distribution, corresponding to equation (19) in the case of INS. For the system consisting of atomic species  $\kappa$  and  $\kappa'$ , a partial structure factor  $S_{\kappa\kappa'}$  is defined as

$$S_{\kappa\kappa'}(Q, \omega) = \frac{1}{N} \sum_{m,n} \int_{-\infty}^{\infty} \langle \langle e^{i\mathbf{Q} \cdot \mathbf{r}_m^\kappa(t)} e^{i\mathbf{Q} \cdot \mathbf{r}_n^{\kappa'}(0)} \rangle \rangle e^{-i\omega t} dt, \quad (27)$$

where  $\langle \langle \dots \rangle \rangle$  means the thermal and orientational average. Using this definition, one has the scattering cross section given by

$$\frac{d^2\sigma}{d\Omega dE} = N r_0^2 (\boldsymbol{\epsilon}_i \cdot \boldsymbol{\epsilon}_f)^2 \frac{k_f}{\hbar k_i} \sum_{\kappa, \kappa'} p_\kappa p_{\kappa'} f_\kappa(Q) f_{\kappa'}(Q) S_{\kappa\kappa'}(Q, \omega). \quad (28)$$

Here  $f_\kappa(Q)$  is the atomic form factor for the species  $\kappa$  and  $p_\kappa$  is its concentration. In the  $Q \rightarrow 0$  limit, the form factor becomes the number of electrons  $Z_\kappa$  of the atom  $\kappa$ . For v-SiO<sub>2</sub>,

$Z_{\text{Si}} = 14$  and  $Z_{\text{O}} = 8$ , and these are actually proportional to the atomic masses  $M_{\text{Si}} = 28$  and  $M_{\text{O}} = 16$ . Therefore, in the small  $Q$ -limit, the scattering cross section for x-rays becomes proportional to the mass density–density correlation function (Ruocco and Sette 2001)

$$\frac{d^2\sigma}{d\Omega dE} = Nr_0^2(\epsilon_i \cdot \epsilon_f)^2 \frac{k_f}{\hbar k_i} S(Q, \omega), \quad (29)$$

with the definition given by

$$S(Q, \omega) = \sum_{\kappa, \kappa'} p_{\kappa} p_{\kappa'} \frac{M_{\kappa} M_{\kappa'}}{M_{\text{tot}}^2} S_{\kappa\kappa'}(Q, \omega). \quad (30)$$

The quantity  $M_{\text{tot}}$  in equation (30) is the total mass of a molecular unit ( $M_{\text{tot}} = 2M_{\text{O}} + M_{\text{Si}}$  for  $v\text{-SiO}_2$ ). The proportionality function between INS and IXS is different, since the thermal neutron scattering lengths are not proportional to the atomic masses as seen from equation (25). The IXS signal at low  $Q$  can be well approximated by the density–density dynamic structure factor, but with increasing  $Q$ , other components, such as the charge–charge dynamic structure factor, start to play a role. The IXS technique is sensitive to the motion of heavier atoms as seen from equation (30). INS does not depend on the number of electrons per atom, but depends purely on a nuclear property. The main difference between IXS and INS is that IXS covers unlimited energy transfers in the accessible  $Q$  transfer range in  $Q$ – $\omega$  space. Provided that the energy resolution is sufficient, the IXS technique becomes a complementary tool to the INS method.

The Brillouin IXS spectra for  $v\text{-SiO}_2$  at  $T = 1055$  K, where the anharmonicity of atomic vibrations become relevant, are illustrated in figure 25 from  $Q = 0.1$  to  $0.4 \text{ \AA}^{-1}$  (Bennasi *et al* 1996, 1997). Bennasi *et al* (1996, 1997), Masciovecchio *et al* (1999) (figure 26) and Pilla *et al* (2000) analysed their data of IXS using the following damped harmonic oscillator (DHO) approximation:

$$F(\omega) = \frac{2}{\pi} \frac{\Omega^2}{(\omega^2 - \Omega^2)^2 + \omega^2 \Gamma^2}, \quad (31)$$

taking the linear dispersion relation  $\Omega = vQ$  with a broadening  $\Gamma$ .

They concluded that the linear dispersion relation of phonon excitations holds up to energies more than twice that of the Boson peak and that these are *propagating* modes. This statement contradicts the finding of the absence of any observable  $Q$ -independent feature at the Boson peak energy (Foret *et al* 1996, Arai *et al* 1999a). The use of the DHO function to fit the spectral density does not indicate any particular physical significance of the nature of the vibrational excitations, since it can equally describe the damped behaviour of a localized mode or of a propagating collective mode. It should be regarded as a suitable empirical function with which to fit asymmetric peaks (Vacher *et al* 1998, 1999).

Foret *et al* (1996) employed the following function in order to analyse their Brillouin IXS and INS. The function is given by

$$F(Q, \omega) = \frac{v^2 Q^2}{\omega^2} \frac{\Gamma}{(\omega^2 + \Gamma^2 - v^2 Q^2)^2 + 4\Gamma^2 v^2 Q^2}, \quad (32)$$

where the width  $\Gamma(\omega)$  takes the form

$$\Gamma(\omega) = \frac{\omega^4}{\omega_0^3} \left[ 1 + \left( \frac{\omega}{\omega_0} \right)^m \right]^{-3/m}, \quad (33)$$

and the frequency dependence of the phonon velocity is defined by

$$v(\omega) = v_0 \left[ 1 + \left( \frac{\omega}{\omega_0} \right)^m \right]^{z/m}. \quad (34)$$

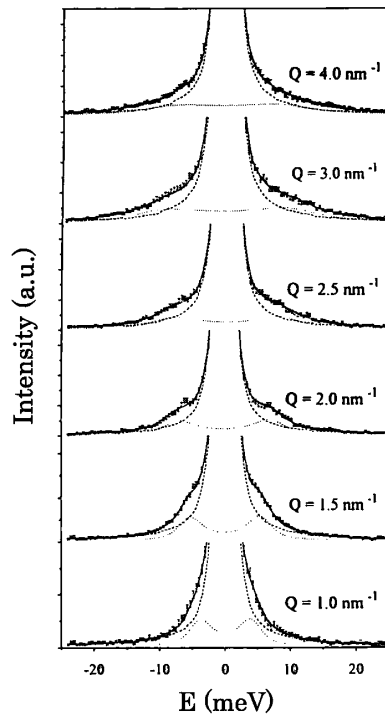


Figure 25. IXS spectra of v-SiO<sub>2</sub> at 1050 K taken at different  $Q$  values. After Bennasi *et al* (1996).

This function was successfully used to analyse the scattering data for sl modes in fractal structures (see, e.g. Nakayama *et al* 1994). The use of a crossover frequency  $\omega_0$  in the function is crucial. Provided that the Boson peak modes consist of sl modes crossed over from extended (ex) acoustic phonons, the use of this type of function is reasonable. From the analysis of the data of Brillouin INS and IXS experiments in terms of the scattering function of equation (32), Foret *et al* (1996) claimed that an acoustic localization edge exists at around 1 THz. We should mention in this respect that Foret *et al* (1997) re-analysed IXS data by Bennasi *et al* (1996) employing the scattering function of equation (32). They demonstrated excellent fits with the IXS data by taking a crossover frequency of  $\nu_0 \approx 1$  THz. Since the interpretation due to the DHO that the Boson peak consists of a propagating acoustic mode is not definite, Foret *et al* (1997) claimed that the propagation of acoustic modes at frequencies beyond the Boson peak of v-SiO<sub>2</sub> is not conclusively demonstrated from IXS experiments.

It should be emphasized again that IXS is sensitive to the motion of Si-atoms. One of the plausible interpretations for the discrepancy between INS and IXS data is that the atomic motions relevant to the flattened dispersion at the Boson peak can be attributed to the motion of O-atoms (Arai *et al* 1999a, Harris *et al* 1999), whereas the linear dispersion above the Boson peak observed by IXS and INS arises mainly from the relative motion of Si atoms.

### 6.3. Crossover to strong scattering of acoustic phonons: Ioffe–Regel criterion

It has been believed that the localization of propagating acoustic phonon yields the universal plateau behaviour in the thermal conductivity of glasses around 10 K. However, the nature of the relation between the Boson peak and the plateau has been controversial. In the early

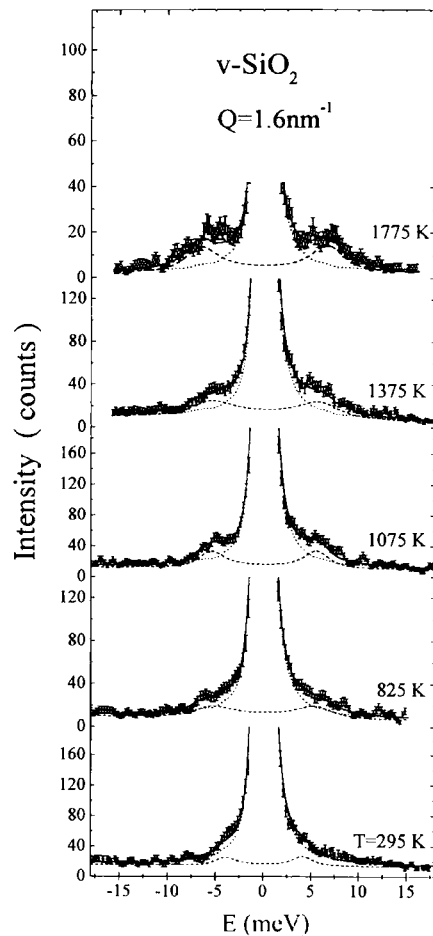


**Figure 26.** IXS spectra of  $\nu$ -SiO<sub>2</sub> at  $Q = 1.6 \text{ nm}^{-1}$  taken at different temperatures. After Masciovecchio *et al* (1999).

stages of the investigations, there were two pictures of the excess Boson peak: one is due to the localization of acoustic phonons by disorder, the other is due to the resonant scattering of acoustic phonons by the local potential. There exists experimental evidence that linear dispersion relations for longitudinal and transverse acoustic waves hold up to the highest measured  $\nu \approx 400 \text{ GHz}$ , and that the linewidth  $\Gamma$  of these waves is proportional to  $\nu^2$  due to internal friction with a temperature dependence (Vacher *et al* 1981, Rothenfusser *et al* 1984, Zhu *et al* 1991, Marath and Maris 1996).

The length scale of domains associated with density fluctuation in  $\nu$ -SiO<sub>2</sub> takes a value of  $R \approx 15 \text{ \AA}$  (Elliott 1991, 1992). Thus, the microscopic structure of  $\nu$ -SiO<sub>2</sub> involves intrinsic structural inhomogeneities owing to density fluctuation domains of diameter  $2R$ . Such density fluctuations strongly scatter acoustic phonons, resulting in a reduction in the mean-free-path  $l_s$  of acoustic phonons. With increasing frequency of the acoustic phonons, the linewidth increases according to the Rayleigh scattering law,  $\Gamma \propto \nu^4$ . This should rapidly yield the strong scattering regime (see figure 18). That is, the Ioffe–Regel (IR) regime under the condition  $\Gamma \approx 2\pi\nu$  holds for  $\nu > \nu_0$ , where  $\nu_0$  is the IR crossover frequency (Ioffe and Regel 1960).

The onset of localization is also expressed, in terms of the IR criterion, as  $ql_s \approx 2\pi$ . The minimum value for  $l_s$  should correspond to the length-scale of domains  $2R \approx 30 \text{ \AA}$  associated with density fluctuations in v-SiO<sub>2</sub>. This value for scattering length  $l_s$  agrees with the mean-free-path calculated using the data for the thermal conductivity of v-SiO<sub>2</sub> (Zeller and Pohl 1971, Graebner *et al* 1986, Vacher *et al* 1997) (see, e.g. figure 18).

One can estimate the mean-free-path owing to the Rayleigh scattering law. This can be obtained by adjusting the following theoretical law

$$l_s^{-1} = Av^4, \quad (35)$$

to the observed mean-free-path  $l_s(\omega)$  of v-SiO<sub>2</sub> given in figure 18. This yields  $A = 9 \times 10^{-2} (\text{\AA}^{-1} \text{THz}^{-4})$ . The substitution of  $v = 1 \text{ THz}$  into equation (35) demonstrates that the mean-free-path becomes of the order of wavelengths of acoustic phonons. This crossover frequency  $\nu_0 \approx 1 \text{ THz}$  coincides with the estimation made in figure 18. Vacher *et al* (1997) found that this Rayleigh scattering should become dominant above about 300 GHz by extrapolating the Brillouin value of the mean-free-path with a  $v^2$  law (see figure 27). Figure 27 shows the inverse mean-free-path  $l_s^{-1}$  against the frequency  $\nu$  of acoustic phonons in v-SiO<sub>2</sub> (Vacher *et al* 1997). Assuming the linear dispersion relation  $q = \omega/v_s$  for acoustic phonons, one has the relation

$$\nu_0 \approx \frac{v_s}{2R}. \quad (36)$$

Thus,  $\nu_0$  should increase with decreasing  $R$ , evidence for which was obtained by Zhu (1994) in the course of thermal conductivity experiments on d-SiO<sub>2</sub>. If the IR criterion due to Rayleigh scattering is the origin of the Boson peak, there should be no temperature dependence of the Boson peak spectra. However, Wischniewski *et al* (1998) found clearly a strong dependence on temperature for the Boson peak spectra. It should be emphasized that there is no excess DOS at the crossover frequency from propagating to localized phonons for the case of fractal

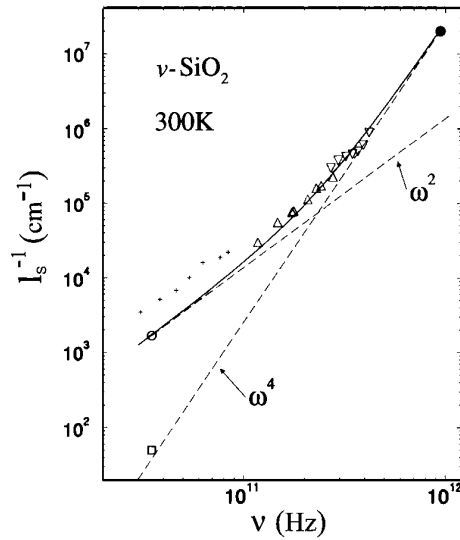


**Figure 27.** Frequency dependence of the mean-free-path  $l_s^{-1}$  for v-SiO<sub>2</sub>. The full black circles are the IR crossover frequency, corresponding to the upper limit of the Rayleigh scattering regime. The  $\omega^2$  line represents the relaxational contribution obtained by the extrapolation of the Brillouin value. After Vacher *et al* (1997).

structures (Yakubo and Nakayama 1987, Bernasconi *et al* 1992). From this, it is natural to conclude that phonon localization is not a necessary condition for the appearance of the excess DOS (the Boson peak). The point is whether or not the onset of localization begins lower than the Boson peak energy. The situation is rather complicated because resonant vibrational states with the length scale of the MRO can become mixed with bare propagating phonon states.

Experimental data on  $v$ -SiO<sub>2</sub> support the conclusion that the Boson peak energy region almost coincides with the crossover frequency  $\nu_0$  of acoustic phonon localization. If the crossover to strong scattering due to Rayleigh scattering occurs at  $\nu_0$  at around 1 THz, the resonant states should be localized above  $\nu > \nu_0$ . If not, the resonant states should be extended. This conclusion is due to the assertion of the non-coexistence of ex and sl modes at the same frequency by Mott and Twose (1961).

Rat *et al* (1999) performed Brillouin XS experiments to observe the crossover frequency  $\nu_0$  to strong scattering of acoustic phonons in  $d$ -SiO<sub>2</sub>. They used  $d$ -SiO<sub>2</sub> to avoid the masking by the wings of the intense elastic signal below about 4 meV. They analysed the data using the function (32) and concluded that longitudinal acoustic phonons are seen up to an energy  $\hbar\omega \approx 9$  meV, corresponding to a scattering vector  $Q \approx 0.22 \text{ \AA}^{-1}$ . At higher  $Q$ , the nature of the signal changed rapidly, indicating a crossover to strong scattering.

This has led to an understanding that local extra-potentials are relevant to the structural origins of both the two-level tunnelling states (TLS) and the sl modes associated with the Boson peak spectrum. The local extra-potentials stemming from internal distortion play a key role in generating the peculiar low-energy dynamics in glasses.

## 7. MD simulations for $v$ -SiO<sub>2</sub>

The first attempt at MD simulations for  $v$ -SiO<sub>2</sub> was made by Bell and Dean (1972) using a hand-made structural model. Later, it became possible to treat more sophisticated models based on simulated structures due to the availability of ever faster computers. Such simulations are likely to play an important role in laboratory experiments. However, for the THz frequency dynamics of glasses, the use of simulated structures is often unjustified due to a number of factors. Binder and Kob (1998) and Horbach *et al* (1999) pointed out several problems with MD simulations on  $v$ -SiO<sub>2</sub>. For MD simulations of realistic systems, the crucial point is the validity of the chosen interatomic potentials and the size of the model. Tsuneyuki *et al* (1988) derived a pair-wise potential by fitting selected *ab initio* calculations, which has been implemented in many MD simulations of  $v$ -SiO<sub>2</sub> (Swaison and Dove 1993, Della-Valla and Venutti 1994, Guillott and Guissani 1997). An improved potential was proposed by van Beest *et al* (1990) and applied to MD simulations of  $v$ -SiO<sub>2</sub> (Vollmayr *et al* 1996, Horbach *et al* 1998). Although these potentials yield structural properties which are consistent with the diffraction data  $S(Q)$ , the agreement with the experimental DOS is less impressive. The best method for creating a realistic structural model for  $v$ -SiO<sub>2</sub> is in *ab initio* Car-Parrinello MD simulations taking account of valence electrons explicitly. Though it is limited to small sizes up to 72 atoms (Sarnthein *et al* 1995a,b, 1997, Pasquarello and Car 1998, Pasquarello *et al* 1998, Pasquarello 2000), the calculated results recover well the dynamic behaviour of  $v$ -SiO<sub>2</sub> above about 5 THz.

Taraskin and Elliott (1997a,b, 1998) have performed MD simulations for  $v$ -SiO<sub>2</sub> employing the two types of potential functions proposed by Tsuneyuki *et al* (1988) and Beest *et al* (1990). The structural models of Taraskin and Elliott (1997a) consist of 216 silicon and 432 O-atoms within a cube of length  $L = 21.4 \text{ \AA}$  with a density  $\rho = 2.2 \text{ g cm}^{-3}$ , employing the periodic boundary condition. The wavelengths of the excited phonons were restricted in the regime  $\lambda < L$ . Assuming the velocity of transverse acoustic phonons to be  $3.74 \times 10^5 \text{ cm s}^{-1}$ ,

one can estimate the minimum frequency of the system as  $\nu_m = 1.78$  THz. This minimum frequency is higher than the main frequency region of the Boson peak of  $v\text{-SiO}_2$  at about 1 THz observed by INS (Buchenau *et al* 1984, 1986) and HRS experiments (Helen *et al* 2000, Yamaguchi and Yagi 1999b). Thus, the results obtained by Taraskin and Elliott (1997a,b, 1998) only partly cover the region of the Boson peak, and similarly for the simulations performed by Horbach *et al* (2001).

The systems employed by Taraskin and Elliott (1997a,b, 1998) were quenched from the liquid state at 5000 K in 100 K steps to the temperature at which atomic diffusion stopped, and then relaxed to a metastable state free of any coordination defects. This showed good agreement with experimental diffraction data on  $S(Q)$ . Their calculated  $Q$ - $\omega$  relation (figure 28) demonstrates the following: (i) Pseudo-periodicity exists for  $k_2 \approx 3 \text{ \AA}^{-1}$ , corresponding to the period of  $d_2 = 2\pi/k_2 \approx 2 \text{ \AA}$  due to the average height of  $\text{SiO}_4$  tetrahedra (see figure 5). (ii) This coincides with the pseudo-periodicity  $2\pi/Q_2$  found from the position of the second sharp diffraction peak at  $Q_2 \approx 3 \text{ \AA}^{-1}$  in  $S(Q)$ . (iii) Another important finding is that the transverse acoustic branch apparently reaches a plateau at  $k_1 \approx 0.7\text{--}0.8 \text{ \AA}^{-1}$ , corresponding to a period of  $d_1 = \pi/k_1 \approx 3.9\text{--}4.4 \text{ \AA}$ . Simulated results suggest that excess modes originate from the lowest optical band states hybridized with transverse acoustic modes.

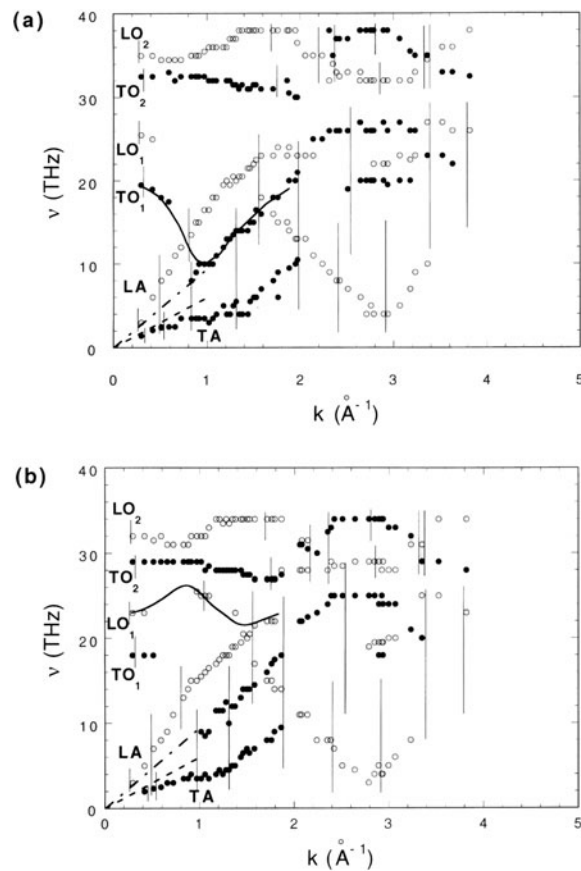


**Figure 28.** Dispersion relations for the structural model of  $v\text{-SiO}_2$  based on (a) the van Beest potential and (b) the Tsuneyuki potential. After Taraskin and Elliott (1997a,b). Vertical bars represent half-widths of the peaks.

Swainson and Dove (1993, 1995) and Dove *et al* (1997) have performed MD simulations for cristobalite and  $v\text{-SiO}_2$  based on a rigid unit model. They claimed that the THz frequency dynamics of  $\beta$ -cristobalite is very similar to that found in  $v\text{-SiO}_2$ . This is due to the existence of rigid-unit modes arising from the underconstrained situation in silica (Thorpe 1983, He and Thorpe 1985). In contrast, a-Si is *overconstrained*, having an average coordination number  $z \approx 2.4$ . This is the reason of the difficulty of achieving double-well potentials in a-Si.

Trachenko *et al* (1998, 2000) performed MD simulations using the split-atom algorithm, in which a strict constraint is assigned to a tetrahedron as a rigid unit (Giddy *et al* 1993). Their structural models consist of defect-free configurations containing 216, 512, and 4096 tetrahedra. Their results show that  $v\text{-SiO}_2$  has the same degree of flexibility as dynamically disordered  $\beta$ -cristobalite (Keen and Dove 1999), which undergoes sudden rotational rearrangement of the structure with little energy cost (Thorpe 1983). For this jump motion the partition ratio indicates that the number of tetrahedra involved is around 30. This suggests the existence of large-amplitude reorientational motions of  $\text{SiO}_4$  tetrahedra, that may be identified as the origin of two-level tunnelling states (TLS) in  $v\text{-SiO}_2$  (Trachenko *et al* 1998).

## 8. Construction of potential functions

### 8.1. Infinitesimal translational and rotational invariance

The difficulty associated with the theory of THz frequency dynamics in glasses lies in constructing the potential functions from a variety of information on the atomic arrangement in glasses. This is a key element to formulate the theory as a starting point for investigation. The appearance of collective modes (phonons) is a consequence of *infinitesimal* translational and rotational invariance (TRI) of the system. This leads to the concept of the zero-frequency mode corresponding to infinitesimal translation as a whole, whose eigenfunction should be orthogonal to all other eigenmodes with finite eigenfrequencies in the system (see figure 29). This follows from the theorem that the modes with non-zero eigenfrequencies are composed of *collectively oscillating* functions even in topologically disordered systems, while the isolated vibrational states of single atoms or groups of atoms do not give a correct picture as in the case of the Einstein oscillator (Einstein 1907). For example, specific heats of insulating crystals drop from a value close to that of  $25 \text{ J mol}^{-1} \text{ K}^{-1}$  at room temperature and approach zero as  $T^3$ , in which crystals' collective modes (acoustic phonons) play a role as explained by Debye (1912).

From a very general point of view, the total potential energy  $V$  of a solid, whether for crystals or glasses, is expressed in terms of a small displacement  $\mathbf{u}_i(t)$  from the equilibrium position of the atom  $i$ , since the potential energy  $V$  should be a function of the instantaneous positions of all atoms (see, e.g. Born and Huang 1954). By expanding in a Taylor series in powers of the atom displacement  $\mathbf{u}_i(t)$  around an equilibrium configuration of the atom at  $\mathbf{r}_i$ , one obtains the Born–von Karman type force-constants from the second-order derivatives

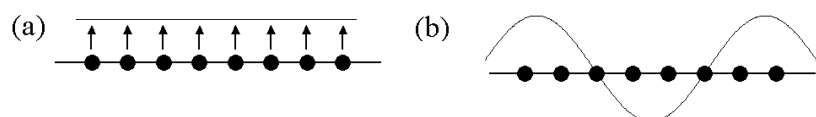


**Figure 29.** Diagrams showing the orthogonality between (a) the infinitesimal translational zero-frequency mode and (b) an excited vibrational mode with finite frequency.

of the potential  $V$  even for glasses with local distortion. However, this type of expansion does not guarantee automatically the TRI of the potential function as a whole. It is more natural to expand the potential function  $V$  in terms of *internal variables* being invariant under translation (T) and rotation (R).

### 8.2. Valence force field in the normalized form

A transparent approach, expanding the potential  $V$  in terms of internal variables such as  $\Delta r_{ij}$ ,  $\Delta \theta_{ijk}$ ,  $\Delta \tau_{ijkl}$ ,  $c$ , is to use the valence force field (VFF) potential, which automatically guarantees the TRI. The VFF was initially introduced to describe vibrations of molecules and later adopted for crystals of diamond structure (Keating 1966) and later applied to chalcogenides (Nakayama and Odajima 1972, 1973). This potential field is the most useful phenomenological description of short-range valence forces and can also naturally describe interatomic interactions governing the bonding which is predominantly covalent. Though the force field can be expressed with the smallest possible number of force constants, its expansion for glasses has nonvanishing terms for *first-order* derivatives associated with tension arising from internal stress. This is the key difference between crystals and glasses.

The VFF potential expressed in terms of internal variables yields

$$\begin{aligned}
 V_{\text{H}}(\dots, r_{ij}, \theta_{ijk}, \tau_{ijkl}, \dots) &= V_0(\dots, r_{ij0}, \theta_{ijk0}, \tau_{ijkl0}, \dots) \\
 &+ \sum \left. \frac{\partial V}{\partial r_{ij}} \right|_0 \Delta r_{ij} + \sum \left. \frac{\partial V}{\partial \theta_{ijk}} \right|_0 \Delta \theta_{ijk} + \dots \\
 &+ \frac{1}{2} \sum \left. \frac{\partial^2 V}{\partial r_{ij} \partial r_{kl}} \right|_0 \Delta r_{ij} \Delta r_{kl} + \frac{1}{2} \sum \left. \frac{\partial^2 V}{\partial \theta_{ijk} \partial \theta_{klm}} \right|_0 \Delta \theta_{ijk} \Delta \theta_{klm} \\
 &+ \frac{1}{2} \sum \left. \frac{\partial^2 V}{\partial r_{ij} \partial \theta_{jkl}} \right|_0 \Delta r_{ij} \Delta \theta_{jkl} \\
 &+ \dots + \text{anharmonic terms,}
 \end{aligned} \tag{37}$$

where  $V_0$  is the static potential energy in a quenched equilibrium state. In equation (37),  $r_{ij0}$ ,  $\theta_{ijk0}$ ,  $\tau_{ijkl0}$   $\dots$  are equilibrium values of the bond length, the bond angle, and the dihedral angle,  $\dots$  defined through the atoms  $i$ ,  $j$ ,  $k$  and  $l$ . The variables  $\Delta r_{ij}$ ,  $\Delta \theta_{ijk}$ ,  $\Delta \tau_{ijkl}$  represent the deviation of the bond length, the bond angle, and the dihedral angle from their equilibrium values. The first-order derivative  $\partial V / \partial r_{ij}|_0 = T_{ij}$  means the *tension* of the bond (that is, the elastic energy per unit length) between the atoms  $i$  and  $j$  at their equilibrium positions.

The tensions  $T_{ij}$  should satisfy the equilibrium condition of forces, namely, the balance of the forces upon the atom because of no flow of atoms in a quenched state (Treloar 1975, Alexander 1998). For example, by writing the tension between the atoms  $i$  and  $j$  as  $T_{ij}$ , the condition of the balance of forces at the atom  $i$  should be expressed as

$$\mathbf{f}_i = \sum T_{ij} \cdot \hat{\mathbf{r}}_{ij} = 0, \tag{38}$$

where  $\mathbf{f}_i$  is the force at the atom  $i$ , and  $\hat{\mathbf{r}}_{ij} = \mathbf{r}_{ij}/|\mathbf{r}_{ij}|$  defined through  $\mathbf{r}_{ij} = \mathbf{r}_i - \mathbf{r}_j$  is the unit vector along the bond  $i$  and  $j$ . In liquid states, the force  $\mathbf{f}_i$  does not vanish. Equation (37) can always be rewritten in bilinear form, taking into account the condition of balance of forces in equation (38), as

$$\begin{aligned}
 \Delta V_{\text{H}}(\dots, \Delta r_{ij}, \Delta \theta_{ijk}, \dots) &= \frac{1}{2} \sum K_{r_{ij}} \left( \Delta r_{ij} + \frac{T_{ij}}{K_{r_{ij}}} \right)^2 \\
 &+ \frac{1}{2} \sum K_{\theta_{ijk}} \left( \Delta \theta_{ijk} + \frac{T_{ik}}{K_{\theta_{ijk}}} \right)^2 + \dots,
 \end{aligned} \tag{39}$$

where  $K_{r_{ij}} = \partial^2 V / \partial r_{ij}^2|_0$ ,  $K_{\theta_{ijk}} = \partial^2 V / \partial \theta_{ijk}^2|_0$ ,  $T_{ij} = \partial V / \partial r_{ij}|_0$  and  $T_{\theta_{ijk}} = \partial V / \partial \theta_{ijk}|_0$ , respectively. The dimension of the ratios  $T/K$  in the parentheses of equation (39) represents that of displacement. Namely, the physical meaning of the terms  $T_{ij}/K_{r_{ij}}$  or  $T_{\theta_{ijk}}/K_{\theta_{ijk}}$  is the displacement of the atom from the position corresponding to the equilibrium bond length and angle due to local internal stresses satisfying the equilibrium condition of the forces (Nakayama 1999). One sees from the normalized potential equation (39) that the same eigenfrequencies and eigenvectors are created as in the case of the potential without the terms of tensions between interacting atoms. As a result, this normalized potential equation (39) rewritten in the *quadratic* form is equivalent to the dynamical system as representing ordinary disordered systems without internal stresses.

### 8.3. Buckling at atomic scales and local extra-potentials

Anderson and Bömmel (1955) were the first to set forth the idea, in order to explain the relaxation process responsible for large acoustic loss, that bent Si–O–Si angles cause two or more equivalent positions around the Si–O–Si straight line and small energy barriers separating the equivalent states. This is natural since the buckling should be produced at the site with small configurational number  $z$ , namely, at the sites of O ( $z = 2$ ) compared with at the sites of Si ( $z = 4$ ) in  $\nu$ -SiO<sub>2</sub>, where buckled atoms are considered to be trapped in one of the double wells. Note that the corresponding potentials are hardened with increasing external pressure, indicating that the Boson peak is very sensitive to pressure as mentioned in section 4.

By introducing a new variable, say, rotational motion of rigid units of tetrahedra, the general form of local extra-potential  $\Delta V_E$  is expressed by

$$\begin{aligned} \Delta V_E(\dots, \Delta Q_{jr}, \Delta Q_{j\theta}, \dots) = & \sum (T_{E_{jr}} \Delta Q_{jr} + \frac{1}{2} K_{E_{jr}} (\Delta Q_{jr})^2 + \frac{1}{3} A_{E_{jr}} (\Delta Q_{jr})^3 \\ & + \frac{1}{4} B_{E_{jr}} (\Delta Q_{jr})^4 + \frac{1}{3} A_{1_{jr}} (\Delta Q_{jr})^2 \Delta r_{ij} + \frac{1}{3} A_{2_{jr}} (\Delta Q_{jr}) (\Delta r_{ij})^2 + \dots \\ & + T_{E_{j\theta}} \Delta Q_{j\theta} + \frac{1}{2} K_{E_{j\theta}} (\Delta Q_{j\theta})^2 + \dots), \end{aligned} \quad (40)$$

where  $\Delta Q_{j\theta} = Q_j - \theta_i$  or  $\Delta Q_{jr} = Q_j - r_i$ . Note that  $\Delta V_E$  satisfies the TRI condition and does not represent isolated potentials. The potential relevant to the two-level-tunnelling states (TLS) with *low-enough* barrier heights should be derived from equation (40), as well as the case of the local extra-potentials for the Boson peak.

The total Hamiltonian satisfying the TRI condition is written as

$$H = \sum_i -\frac{\hbar^2}{2m_i} \nabla_i^2 + \Delta V_H + \Delta V_E, \quad (41)$$

where  $\Delta V_H$  is a usual quadratic form of the potential given by equation (39). Each potential plays a role for creating the peculiar dynamics at THz frequencies and below.

Recently, Nakamura *et al* (2002) have performed INS measurements for  $\nu$ -SiO<sub>2</sub>,  $d$ -SiO<sub>2</sub>,  $\alpha$ -cristobalite and  $\alpha$ -quartz to obtain the averaged mean-square displacements through an evaluation of the Debye–Waller factor. They found clear evidence that the averaged mean-square displacement relevant to the Boson peak of  $\nu$ -SiO<sub>2</sub> are especially large at any temperature from 20 to 300 K, indicating that anharmonic potentials in  $\nu$ -SiO<sub>2</sub> such as double-well potentials with small barrier heights give rise to an excess DOS at around 5 meV, namely, the Boson peak.

### 8.4. $T$ -linear specific heat below 1 K

Phillips (1972) and Anderson *et al* (1972) have postulated the existence of isolated asymmetric double-well potentials with low-enough barrier heights and short-enough distance, ignoring

the coupling with the vibrations of surrounding atoms. That is, their double-well potentials do not satisfy the TRI condition. In the following we give the reason why this simplified approach was successful in describing the phenomena observed below 1 K.

Acoustic phonons excited at low temperatures below 1 K have wavelengths longer than about 2500 Å when taking the sound velocity  $v_s \approx 5 \times 10^5 \text{ cm s}^{-1}$ . These wavelengths are longer than the length scales of the local extra-potential  $\Delta V_E$  that is spatially localized in the 10 Å range. This is one of the reasons why the adiabatic approximation for TLS is valid for local extra-potentials expressed by asymmetric double-well potentials reflecting the microscopic buckling, where the potential barrier-height and the separation of the two local minima are distributed according to such factors as the particular configuration of atoms surrounding the two minima and the internal stresses.

The number density  $n_0$  of the two-level-systems (TLSs) can be estimated using the following theoretical expression for the  $T$ -linear specific heat (Anderson *et al* 1972, Phillips 1972).

$$C(T) = \left(\frac{\pi^2}{6}\right) n_0 k_B^2 T. \quad (42)$$

By substituting the observed magnitude of the specific heat of v-SiO<sub>2</sub> into this, one has the number density  $n_0$  contributing to the TLS as  $n_0 \sim 1/250$  of the total number of SiO<sub>4</sub> groups. The TLS model (corresponding to a *para* state without correlation between TLSs) describes the thermal properties of glasses at low-temperatures, but not the properties at *very* low temperatures around the mK temperature region where the interaction between TLSs via elastic or electric dipole interactions become relevant. A characteristic temperature  $T_c$  is estimated from elastic dipole interactions of the form  $g/r^3$ , taking the average distance of TLS's  $r \approx 100 \text{ Å}$  and the coupling constant  $g \approx 10^4 \text{ K Å}^3$  (Carruzzo *et al* 1994). The frozen-in state of TLSs should be realized at *very* low temperature as a correlated configuration due to interactions between TLSs, which should yield different features in thermal properties from those observed in the temperature range 0.01–1 K (Rogge *et al* 1996, 1997a,b, Strehlow *et al* 1998, Hunklinger *et al* 1999, Kettemann *et al* 1999). It will be possible, due to interactions between TLSs, to realize a *macroscopic quantum state* ( $S_0 = 0$ ) as  $T \rightarrow 0$  according to the *Nernst theorem*. All of these features mentioned above are derived in principle from the local extra-potential equation (40) which fulfils the TRI condition incorporating the coupling with surrounding atoms.

### 8.5. Relevance to the soft potential model

Karpov *et al* (1983) and Karpov and Parshin (1985) introduced the concept of the soft-potential model (SPM) for describing THz frequency dynamics in glasses. See, for a review, Parshin (1994). The isolated SPM is really derived under an *adiabatic* approximation neglecting the coupling with vibrations of surrounding atoms, which does not satisfy the TRI condition.

We describe the physical implications of the SPM. Expressing the amplitude of vibrational motions of atoms or groups of atoms in an extra-potential and that of surrounding atoms as  $Q$  and  $q$ , respectively, one has the relation  $K_E \langle Q^2 \rangle \approx K_r \langle q^2 \rangle \approx k_B T$  at the temperature  $T$  from the principle of equipartition of energy, where  $\langle \dots \rangle$  means the thermal average. In the case that the force constant  $K_r$  is larger than the force constant of the extra-potential  $K_E$ , that is,  $K_r \gg K_E$ , one has the relation  $\langle Q^2 \rangle \gg \langle q^2 \rangle$ . Namely, the amplitudes of surrounding atoms are small compared with that of atoms or groups of atoms in the extra-potential. This makes us approximate equation (40) by neglecting the contribution of displacements of surrounding

atoms as

$$\Delta V_E = \sum \left( \frac{1}{2} K_{E_i} Q_i^2 + \frac{1}{3} A_{E_i} Q_i^3 + \frac{1}{4} B_{E_i} Q_i^4 + \dots \right). \quad (43)$$

Although equation (43) is a crude approximation, it is possible to analyse numerous experimental data by means of parameter fitting (Karpov *et al* 1983, Karpov and Parshin 1985).

## 9. Model Hamiltonians reduced to the harmonic form

When describing the *non-adiabatic* effect, it is fruitful to reduce the potential to a simple one, namely, by adopting a quasi-harmonic approximation. For this quadratic form of the Hamiltonian, the main problem is reduced to that of obtaining eigenfrequencies  $\omega_i$  by solving a set of classical equations of motion and their eigenvectors. This approach has been adopted by several authors.

Laughlin and Joannopoulos (1977, 1978) presented a theory of atomic vibrations of  $v\text{-SiO}_2$  based on the Bethe lattice model. They focused their attention on the role of the Si–O–Si angle distribution in the relatively high frequency regime. Properties of phonons in  $v\text{-SiO}_2$  are classified into those arising from short-range-order and to the disruptive effects of the Si–O–Si bond angle disorder. Their results supported the viewpoint that rocking and bending can be distinguished from one another only by the presence of a Si–O–Si bend of about  $145^\circ$ . It is surprising that the spectrum higher than 3 THz was described well by this simplified model. The effects of the angular force constant ( $K_\theta$ ) are crucial, giving rise to the softening of the rocking bands. These bands (the Boson peak) are predominantly angle-distorting vibrations and are sensitive to changes in the angular force constant. Namely, these are sensitive to external pressure. The results provide important insights: (i) The dynamic properties  $v\text{-SiO}_2$  in the THz frequency region are completely dominated by local effects, particularly the values of the bond angles. (ii) The bond-angle distribution is important in that it broadens features in the spectrum. (iii) The topology of  $v\text{-SiO}_2$  is not manifested in the relatively high frequency regime.

The sensitivity of the DOS to very large Si–O–Si bond angle distortions was investigated by Sen and Thorpe (1977). They proposed a theoretical framework for the study of the vibrational properties of  $v\text{-SiO}_2$  using the VFF model, leading to the concept of floppy modes.

Schirmacher *et al* (1998) and Akita and Ohtsuki (1998) have investigated a three-dimensional (3d) simple-cubic system governed by a coupled harmonic model with a random distribution of force constants. They have found quite naturally an excess Boson peak compared to the Debye behaviour in the DOS. The point of their result is that relevant modes for the Boson peak are not localized, as evidenced by an analysis of the level-distance-statistics of the spectra. This conclusion seems to be attributed to their use of a simple-cubic model with only one length scale  $a_0$  of the lattice spacing, which makes the crossover frequency  $\nu_0$  to localization at much higher frequencies than the eigenfrequencies corresponding to the Boson peak. This makes it possible for the modes relevant to the Boson peak not to be localized.

We should emphasize that localized resonant modes do not coexist with ex (propagating/acoustic) modes at the same eigenfrequency  $\omega$ , according to the conjecture of Mott and Twose (1961). This is because the eigenfrequencies of the resonance states due to local extra-potentials are embedded in the continuous band of ex acoustic modes. However, provided that the onset of localization of acoustic modes occurs below these resonance frequency distributions arising from the local extra-potentials, the existence of sl modes is guaranteed. Thus, it is necessary in order to have sl modes that the onset of phonon localization

occurs below these resonance frequencies. For v-SiO<sub>2</sub>, the IR criterion yields the crossover frequency from extended to localized acoustic phonons at  $\nu_0 \approx 1$  THz as mentioned in section 7. This condition is automatically satisfied in the case of a one-dimensional (1d) disordered system from the theorem of Anderson localization, stating that all excited modes are weakly localized in 1d systems and have a *discrete* eigenfrequency distribution. Anderson localization of phonons in ordinary disordered systems depends on the dimensionality (Abrahams *et al* 1979, John *et al* 1983). In contrast, the appearance of the Boson peak seems not to depend on the dimensionality of the system as observed in 1d polymer glasses (Kanaya *et al* 1988), folded proteins (Brown *et al* 1972, Genzel 1976, Cusack and Doster 1990, Leyser *et al* 1999), and 2d systems such as a-GeS<sub>2</sub> (e.g. Yamaguchi *et al* 1999a), indicating that the Boson peak has a quite different origin from that of Anderson localization.

The physical model proposed by Nakayama (1998a,b, 1999) represents a possible glassy state in a local minimum on the potential map in configuration space. Its topological feature of *two length scales* for the nearest neighbour distance  $a_0$  and the average size of network unit  $L$  is taken into account as shown in figure 30. This model consists of two main chains with a constant mass  $M$  of molecular units (tetrahedra), and these are connected to their nearest neighbours by linear springs with constant strength  $k$ . The central hypothesis of the model is that there should be a certain number of local extra-vibrational states, which are attached to each chain by linear springs with strength  $K_j$  at site  $j$  with mass  $M$ . The mass  $M$  and the force constant  $K_j$ , where strength is of the order of bending or torsional force constant  $K_\theta$  or  $K_\phi$  (see figure 8), are related to the characteristic frequency  $\omega_j^2 = K_j/M$  of these

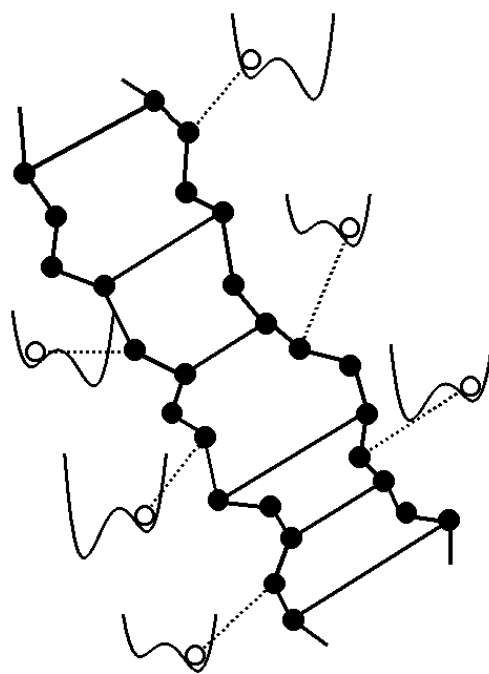


**Figure 30.** Schematic illustration of a physical model for network glasses in the centre-of-mass system. The network structure is composed of unit cells with randomly distributed six or eight molecular units (of 6- or 8-membered rings). The open circles represent a group of atoms trapped in extra-potentials arising from internal strain, which are randomly attached to the two main chains. After Nakayama (1998).

additional states, where the parameters  $\omega_j^2$  are random quantities and assumed to be uniformly distributed in the range between  $\omega_{\min}^2$  and  $\omega_{\max}^2$ . We should emphasize that molecular units connected by the spring constant  $K_j$  in figure 30 do not directly correspond to the true molecular arrangement in v-SiO<sub>2</sub>. It simply refers to some kinds of low-energy vibrational states. It is not worthwhile giving a strict picture for these entities since it depends on such factors as the particular configurations of the molecular units surrounding the local extra-vibrational states.

The Hamiltonian is expressed by

$$H_R = \sum_{i,j} \left( \frac{p_i^2}{2M} + \frac{P_j^2}{2M} + \frac{k}{2}(q_i - q_{i-1} + t_i)^2 + \frac{K_j}{2}(Q_j - q_i + u_i)^2 \right), \quad (44)$$

where the molecules have mass  $M$ ,  $Q_i$ , and  $q_i$  are generalized coordinates representing displacements or changes of angle variables. The corresponding momenta are denoted by  $P_i$  and  $p_i$ , respectively. Lower letters denote quantities for the backbone network structure and capital letters correspond to additional vibrations arising from extra-potentials. The symbols  $t_i$  and  $u_i$  express random displacements due to internal stress satisfying the balance of forces in equation (44). Though the phonon field is recognized as vector in nature, vibrations lose their pure longitudinal and transverse character in glasses, so that a scalar model can be expected to capture the essential features of the THz frequency dynamics of glasses. One sees, by fixing the displacement of  $q_i$  of surrounding neighbours, that the reduced Hamiltonian equation (44) gives rise to the adiabatic extra-potential equation (43) under the quasi-harmonic approximation. This model provides a useful conceptual framework within which to discuss some of the dynamic properties at THz frequencies of v-SiO<sub>2</sub>. The key point of this quasi-1d model is that long-wavelength acoustic modes are weakly localized already; namely, the onset frequency corresponding to the Anderson localization is at  $\nu_0 = 0$ , which makes it possible to have sl modes due to extra-potentials (see figure 31). Using a numerical method called the forced oscillator method (see, e.g. Nakayama and Yakubo 2001),  $S(Q, \omega)$  were calculated for the system size  $N = 14\,000$  in units of  $M = 1$  and  $k = 1$  in figure 32, where periodic boundary conditions are taken and the orientational average is not performed. We have assumed a uniform distribution of the frequency  $\omega_j = \sqrt{K_j/M}$  between  $\omega_{\min} = \frac{1}{4}$  and  $\omega_{\max} = 1$ . In addition, the force constant  $K_j$ , primarily representing a bending or torsional force constant  $K_\theta$ , should be smaller than  $k$ .

An important conclusion drawn from figure 32 is that there clearly appear two bands in the calculated spectra. The lower peaks, with widths moderately increasing with wave number  $Q$ ,

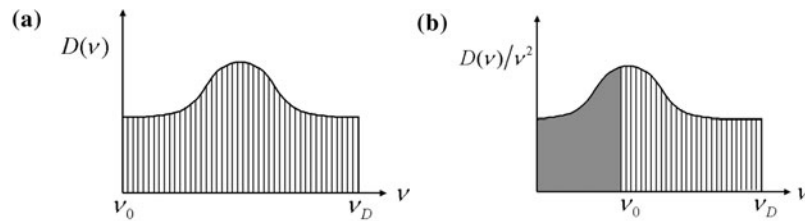


**Figure 31.** Schematic illustration of the role of the onset frequency  $\nu_0$  for the localization of the modes relevant to the Boson peak. (a) The resonance frequencies stemming from extra-potentials are embedded in discrete spectra in a 1d disordered system. Note that  $\nu_0 = 0$  for a 1d disordered system in the sense of the Anderson localization. (b) The 3d case where the onset frequency  $\nu_0$  exists in the excess DOS. A part of the modes stemming from extra-potentials are localized, while others are delocalized in the continuous band.

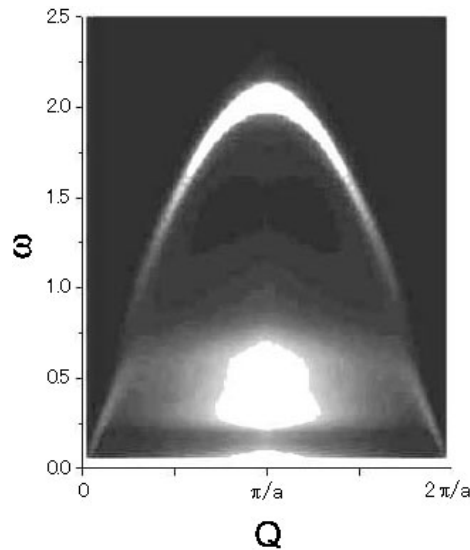


**Figure 32.** Calculated  $S(Q, \omega)$  with the total site number  $N = 14000$ . Characteristic frequencies  $\omega_i$  are distributed between  $\omega_{\min} = \frac{1}{4}$  and  $\omega_{\max} = 1$ . The system of units used is  $M = k = a = 1$ . After Nakayama (1999).

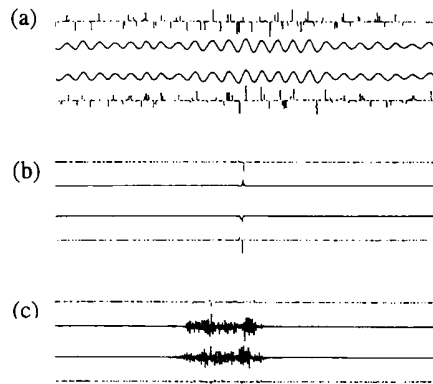


**Figure 33.** Three types of mode patterns: (a) weakly, (b) strongly, and (c) intermediately localized modes. The upper and lower plots in each panel show the displacements of side atoms. The displacements of the main chains are given in the two central curves in each panel. (a) The eigenmode with the eigenfrequency  $\omega = 0.199038$ . (b) The eigenmode with  $\omega = 0.599734$ . (c) The eigenmode with  $\omega = 1.91154$ . After Nakayama and Sato (1998).

are almost independent of  $Q$  (non-dispersive). The peak of the higher band depends strongly on  $Q$ , indicating that the contributing modes are *dispersive* and reflect the short range order in network glasses.

Figure 33(b) shows the eigenmode with  $\omega_\lambda = 0.6770319$  which provides evidence of sl modes in the frequency region  $\omega_{\min} < \omega < \omega_{\max}$ . It should be noted that atoms in extra-potentials and atoms belonging to main chains vibrate in *antiphase optic modes*. The strong localization in the range  $\omega_{\min} < \omega < \omega_{\max}$  arises from the resonance between excitations along main chains and extra-vibrational states. Thus, the distributed  $\omega_i$  is the key element for the strong localization. Figure 33(c) is the eigenmode with  $\omega_\lambda = 1.7095462$  belonging

to the higher band. The mode pattern possesses quite different characteristics from those given in figures 33(a) and (b), indicating that only atoms in main chains vibrate significantly, and atoms belonging to extra-potentials do not follow the vibrations of the atoms in the main chains. In addition, these modes are dispersive and intermediately localized. These two features have been demonstrated by the high-flux and high-resolution INS experiments of Arai *et al* (1999a,b) (see figures 22 and 23). In particular, the feature on the intermediately localized modes, associated with the vibrations of the main chains, is responsible for the existence of the dispersive modes above the Boson peak (Bennasi *et al* 1996, Arai *et al* 1999a). It should be noted that this characteristic is well reproduced (Nakayama 1998a,b) in the calculated  $S(Q, \omega)$  as shown in figure 32.

As shown in figure 32, though there exist *dispersive* modes above the Boson peak spectrum, these are intermediately *localized* and constitute the part of the broad second band in RS experiments, for example, at around  $450 \text{ cm}^{-1}$  for v-SiO<sub>2</sub> (Winterling 1975). These modes are not propagating, but rather, dispersive optic modes. This view is consistent with the evidence from thermal conductivity measurements  $\kappa(T)$  for v-SiO<sub>2</sub> (Zeller and Pohl 1971), which show the temperature-independent plateau at the Boson-peak frequencies and the subsequent rise of  $\kappa(T)$  *proportional to T*, which cannot be explained by assuming the existence of propagating modes. These experimental features are in conflict with the assignment of the Boson peak spectrum as being due to propagating modes at around/above the Boson peak spectrum. We emphasize again the non-coexistence of ex (propagating) and localized modes at the same frequency (Mott and Twose 1961).

To summarize, the reduced Hamiltonian (Nakayama 1998a,b) for the so-called Boson peak ascribes this feature to a sl mode of optic mode character, with an energy and a length scale characterized by density fluctuation domain due to ring size distribution (see figure 30). Below this band, the vibrational states are found to be extended; above this band they are found to be intermediately localized (ml) and dispersive, with length scales of the order of  $10\text{--}100a_0$ . These recover well the experimental features of the vibrational modes in v-SiO<sub>2</sub>.

## 10. Heat transport due to the hopping of sl modes

The thermal conductivity of glasses exhibits a broad, temperature-independent plateau at around 10 K and, shows approximately linear behaviour at high temperatures (Zeller and Pohl 1971, Cahill and Pohl 1987, Cahill *et al* 1992), as shown in figure 2. Thermal conductivities proportional to  $T^2$  below 1 K have been interpreted by postulating TLS (Anderson *et al* 1972, Phillips 1972). The plateau is caused by the onset of acoustic phonon localization at around  $\nu_0 \approx 1 \text{ THz}$ ; namely, heat transport can only occur via already excited ex phonons below  $\nu_0$ . Such behaviour leads to a saturation in  $\kappa(T)$  referred to as the plateau. In other words, the contribution to  $\kappa(T)$  from ex phonon sources will saturate as in the case of the specific heat in the Dulong–Petit regime. The region in which  $\kappa(T)$  is linearly proportional to  $T$  (Cahill and Pohl 1987, 1992) above 10–30 K is much less well clarified (see figure 34). Nakayama and Orbach (1999) have explained quantitatively the rise of the thermal conductivity  $\kappa_{\text{hop}}(T)$  above the plateau temperature region in terms of the ex phonon-assisted-hopping mechanism of the sl modes, which will be described below.

### 10.1. Anharmonic interaction between sl modes and propagating acoustic phonons

The extra-potential  $\Delta V_E$  should possess a large anharmonicity according to the experimental evidence of RS under pressure (Hemley *et al* 1986, Yamaguchi *et al* 1998, Yamaguchi and Yagi 1999a). Use of these measurements enables us to calculate quantitatively

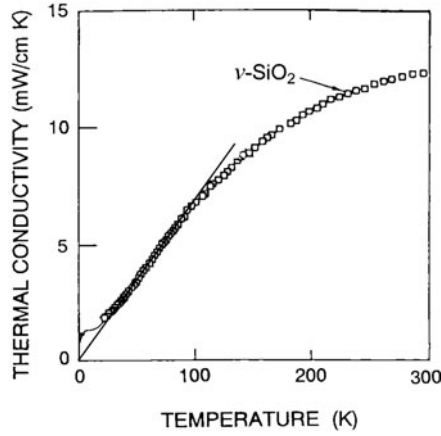


**Figure 34.** Thermal conductivities for temperatures above the plateau for v-SiO<sub>2</sub>. The straight line is drawn as a guide to the eye. After Cahill and Pohl (1987).

$\kappa_{\text{hop}}(T)$  by virtue of propagating phonons (ex) assisted by vibrational hopping of the sl modes.

The most important anharmonic interaction arises from the term  $(\frac{1}{3})A_{1jr}(\Delta Q_{jr})^2\Delta r_{ij}$  in equation (40), where  $\Delta Q_{jr}$  represents a variable associated with the sl mode and  $\Delta r_{ij}$  that of the acoustic (ex) modes. The continuous version of this anharmonic interaction is given with the definition of the third-order elastic stiffness coefficient as

$$V_A = C_{\text{eff}} \int (\nabla \cdot \mathbf{u})^3 d\mathbf{r}, \quad (45)$$

where the atomic displacement  $\mathbf{u}(\mathbf{r})$  is given by equation (21). The respective wavefunctions in equation (21) can be expressed as  $\varphi_{\lambda}^{\text{ex}}(\mathbf{r}) = \sqrt{1/V}e^{i\mathbf{k}_{\lambda} \cdot \mathbf{r}}$  for the ex  $\lambda$ -mode, and  $\varphi_{\lambda'}^{\text{sl}}(\mathbf{r}) = \sqrt{1/\pi l_{\lambda'}^3}e^{-r/l_{\lambda'}}$  for the sl  $\lambda'$ -mode with the localization length  $l_{\lambda'}$ . Substituting this into equation (45), we have the second quantized anharmonic potential of the form

$$V_A = C_{\text{eff}} \sum_{\lambda, \lambda', \lambda''} A_{\lambda\lambda'\lambda''} (b_{\lambda}^{\dagger} b_{\lambda'} b_{\lambda''} + \text{h.c.}). \quad (46)$$

The explicit form for the coupling constant is given by

$$A_{\lambda\lambda'\lambda''} = \sqrt{\frac{1}{V}} \left( \frac{\hbar}{2\rho} \right)^{3/2} \left( \frac{\omega_{\lambda}}{\omega_{\lambda'}\omega_{\lambda''}} \right)^{1/2} \frac{I}{v_s l_{\lambda'} l_{\lambda''}}. \quad (47)$$

Here,  $\rho$  is the mass density,  $v_s$  the velocity of sound and  $V$  the volume, respectively. The factor  $I$  is given by

$$I = \int d\mathbf{r} e^{i\mathbf{k} \cdot \mathbf{r}} \varphi_{\lambda'}(\mathbf{r}) \varphi_{\lambda''}(\mathbf{r}) \approx \left( \frac{16}{\pi} \right) e^{-R_{\lambda'}/l_{\lambda'} + i\mathbf{k} \cdot \mathbf{R}_{\lambda'}}, \quad (48)$$

where  $\varphi_{\lambda'}(\mathbf{r})$  represents the exponentially damped wave function for the sl mode  $\lambda'$ , and  $R_{\lambda'}$  is the hopping distance associated with the sl mode  $\lambda'$ . To derive this, we have pulled out  $e^{i\mathbf{k}_{\lambda} \cdot \mathbf{r}}$  from the integral by the use of  $e^{i\mathbf{k}_{\lambda} \cdot \mathbf{R}_{\lambda'}}$ . This is because the wave number  $\mathbf{k}_{\lambda}$  for ex-phonons is much smaller than that for sl modes with  $k_{\lambda} r \ll r/l_{\lambda'}$ .

The thermal conductivity arising from the vibrational hopping mechanism is given by (Alexander *et al* 1986)

$$\kappa_{\text{hop}}(T) = \frac{k_B}{2V} \sum_{\lambda'} \frac{R^2(\omega_{\lambda'})}{\tau_{\text{sl}}(\omega_{\lambda'}, T)}, \quad (49)$$

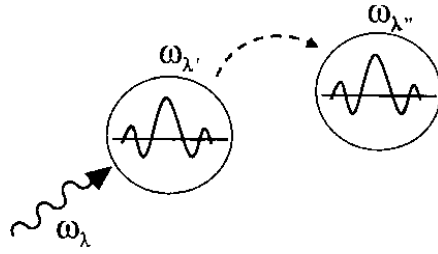


**Figure 35.** Schematic illustration of the first-order process for the sl mode contribution to heat conduction. An ex mode ( $\omega_{\text{ex}} < \omega_0$ ) is denoted by a wavy line, while an sl mode ( $\omega_0 > \omega_{\text{ex}}$ ) is denoted by a circle. Schematic illustration of the hopping transport of an sl mode due to a first-order process. A ex mode is denoted by a wavy line. After Nakayama and Orbach (1999).

where  $R(\omega_{\lambda'})$  is the hopping distance associated with the sl mode  $\lambda'$ , and  $\tau_{\text{sl}}(\omega_{\lambda'}, T)$  is the hopping life-time of the sl mode  $\lambda'$  caused by anharmonic interactions at temperature  $T$ , and  $V$  is the volume of the system (see figure 35). The temperature range over which equation (49) is evaluated includes the Boson peak frequency region. However, inherent localization of the modes above the Boson peak frequency does not allow them to contribute directly to  $\kappa(T)$ .

First-order perturbation theory gives the formula,

$$\frac{1}{\tau_{\text{sl}}(\omega_{\lambda'}, T)} = \frac{2\pi}{\hbar^2} \sum_{\lambda\lambda''} |C_{\text{eff}}|^2 |A_{\lambda,\lambda',\lambda''}|^2 [1 + n(\omega_{\lambda}) + n(\omega_{\lambda''})] \delta(\omega_{\lambda} + \omega_{\lambda''} - \omega_{\lambda'}), \quad (50)$$

where  $n(\omega_{\lambda})$  is the BE factor for the  $\lambda$  mode. The volume which contains at least one sl mode is given by

$$\frac{4\pi}{3} D(\omega_{\lambda'}) \omega_0 [R(\omega_{\lambda'})]^3 = 1, \quad (51)$$

where  $\omega_0$  is the crossover frequency to localization and  $D(\omega_{\lambda'})$  is the density of sl states per unit energy. This condition ensures that, for an sl mode at the origin, a second sl mode can be found within a (hopping) distance  $R(\omega_{\lambda'})$ .

Inserting  $R_{\lambda'}$  from equation (51) into equation (50) and evaluating the double sum, one finds,

$$\frac{1}{\tau_{\text{sl}}(\omega_{\lambda'}, T)} = \frac{32C_{\text{eff}}^2 k_{\text{B}} T}{\pi^3 v_s^5 \rho^3 l_{\lambda'}^4} \left( \frac{\omega_0}{\omega_{\lambda'}} \right)^2 e^{-a\omega_{\lambda'}/\omega_0} \quad (52)$$

where  $v_s$  is the speed of sound. Using the definition,

$$\sum_{\lambda'} = \frac{3V}{\xi_M^3} \int_{\omega_0}^{k_{\text{B}}T/\hbar} \frac{d\omega_{\lambda'}}{\omega_0}, \quad (53)$$

where  $\xi_M^3$  is the volume for finding a single sl mode, the hopping contribution to the thermal conductivity from equation (49) becomes, to within factors of order unity,

$$\kappa_{\text{hop}}(T) = \frac{4^3 3 C_{\text{eff}}^2 k_{\text{B}}^2 T}{\pi^3 v_s^5 \rho^3 \xi_M^3 \bar{l}_{\lambda}^2}, \quad (54)$$

where  $\bar{l}_{\lambda}$  is the average sl length scale of the mode  $\omega_{\lambda}$ . Another derivation of equation (54) is given in the paper by Nakayama (1999). Equation (54) has very few undetermined parameters. An analysis of scattering experiments and specific heat data indicates that the number density of the sl mode should be about 10–20% of the total number density of acoustic modes (Sokolov *et al* 1993). By taking the number of sl modes to be about unity, within a volume  $\xi_M^3$ , this number density leads to the length scale  $\xi_M$  introduced here of the same order of the length scale of domains of density fluctuation 15 Å for v-SiO<sub>2</sub> (Elliott 1991).

Using the value of the anharmonic coupling equation (40) by Yamaguchi and Yagi (1999a) to calculate the sl contribution to  $\kappa_{\text{hop}}(T)$  for a-GeS<sub>2</sub>, one has,

$$\kappa_{\text{hop}}(T) \approx 0.0065T \text{ W mK}^{-1}, \quad (55)$$

using the known parameters for a-GeS<sub>2</sub>:  $v_s = 2030 \text{ m s}^{-1}$ ,  $\rho = 2.72 \text{ g cm}^{-3}$ , and  $\xi_M = 15 \text{ \AA}$ . This contribution to  $\kappa(T)$  is quite comparable to that required for other network forming glasses above the plateau value. For example, for v-SiO<sub>2</sub>, one requires an additional contribution above the plateau,  $\kappa(T) \approx 0.006T \text{ (W mK}^{-1})$  (Cahill and Pohl 1987, 1992), quite close to that calculated for a-GeS<sub>2</sub> using the anharmonic coupling appropriate to the sl modes.

Using the above values for the parameters for a-GeS<sub>2</sub>, one finds at  $T = 10 \text{ K}$ ,

$$\omega_{\text{ex}} \tau_{\text{sl}}(\omega_{\text{sl}}, T) \approx 2-3, \quad (56)$$

showing that our calculation is self consistent. The linear temperature dependence of  $1/\tau_{\text{sl}}$  and equation (54) show that quantum effects will set in just in the range where they are observed. Beyond this temperature regime, one can no longer use equation (54) but must put in the finite life time of the sl mode into the delta function in equation (50). As Simons (1964) showed, this leads to the hydrodynamic or Akhieser limit for vibrational scattering.

A possibility is that the ml modes could interact anharmonically with themselves, thereby, contributing to heat conduction above the plateau. However, such contributions would be small because again  $C_{\text{MMM}} \approx C_{\text{PPP}} \ll C_{\text{SSP}}$ . Further, such processes would yield a much stronger power dependence on  $T$  or a temperature dependence appropriate to Umklapp processes if the high frequency modes were extended (see, e.g. Landau and Lifshitz 1979).

The analysis given here leads to the following interpretation of  $\kappa(T)$  for network glasses as exhibited in figure 2: (i) at low temperatures, the ex modes are scattered by the two level systems (TLS), and  $\kappa(T) \propto T^2$ , (ii) at higher temperatures (the plateau region) the ex modes are exhausted at a crossover frequency  $\omega_0$  associated with the sl modes, leading to  $\kappa(T) = \text{const.}$ , the Dulong–Petit limit, and (iii) at temperatures above the plateau an additional channel associated with sl mode hopping becomes important, accounting for the increase in  $\kappa(T) \propto T$  above the plateau temperature. In addition, (iv) the *curving over* of the last contribution as  $T$  continues to increase arises from the quantum condition,  $\omega_{\text{ex}} \tau_{\text{sl}} \approx 1$  (Simons 1964).

## 11. Conclusions

The frequency range of around 1 THz of the Boson peak, i.e. the excess contribution to the usual Debye DOS, is almost the same as the relevant frequencies associated with the plateau in the thermal conductivity of v-SiO<sub>2</sub>. These two features observed by different measurements, spectroscopy, and heat transport, are universal phenomena in network glasses, and appear to be insensitive to the chemical composition of covalently bonded network glasses. The universality of these phenomena has proved to be a great attraction for physicists and chemists who strive to provide a unified picture of the THz frequency dynamics of network glasses.

In this paper, we have critically examined various approaches by raising the following questions: What is the mechanism for the onset of the plateau in thermal conductivities? Is the Boson peak directly related to the plateau in thermal conductivities? Why is the Boson peak sensitive to pressure as well as the FSDP? Why does the Boson peak in d-SiO<sub>2</sub> diminish and shift to higher frequencies? What modes are relevant to pseudo-phonon dispersion above the Boson peak? Why does the Boson peak possess a flat dispersion independent of  $Q$ ? What is the origin of the linear rise of  $\kappa(T)$  with  $T$  above the plateau? Explanations for these questions are given below.

There are two important length-scales in  $v\text{-SiO}_2$ . One is the medium-range order between a  $\text{SiO}_4$  tetrahedron and the other the correlation length  $R$  owing to density fluctuation domains associated with the ring-size distribution. The plateau in thermal conductivity  $\kappa(T)$  of  $v\text{-SiO}_2$  is the consequence of a crossover from extended to localized vibrational excitations. The length scale  $R$  of domains plays a key role in the onset of the phonon localization as concluded from an analysis of the IR criterion. It is crucial for the case of  $v\text{-SiO}_2$  that the crossover from ex to localized modes occurs where the wavelength  $\lambda(\omega_0)$  of propagating acoustic phonons becomes of the order of the length scale  $R$  of domains.

The onset of the localization of acoustic phonons is not a necessary condition for yielding the excess contribution to the DOS, the Boson peak, as demonstrated in the case of the phonon–fracton crossover (Yakubo and Nakayama 1987). It is not necessary that the modes relevant to the excess contribution to the DOS are localized. However, the onset of localization is a necessary condition for the appearance of the plateau in the thermal conductivity. The point is that the onset of acoustic phonon localization due to the IR criterion is located in almost the same energy region of the excess DOS, the Boson peak, in the case of  $v\text{-SiO}_2$ . This coincidence in energy scale is the reason why the excess modes due to local extra-potentials relevant to the Boson peak are sl. This is a manifestation of the conjecture of Mott and Twose (1961), stating that the coexistence of localized and ex modes at the same eigenfrequency is not allowed (see figure 32).

As shown by means of HRS experiments (Yamaguchi and Yagi 1999b, Helen *et al* 2000), the Boson peak for  $v\text{-SiO}_2$  mainly consists of the lowest transverse optic modes associated with the coupled rotational motions of tetrahedra (Buchenau *et al* 1984, 1986). Relevant modes should be sl in local potentials satisfying the TRI and be hybridized with transverse acoustic phonons (Nakayama 1998, Nakayama and Sato 1998). Another important feature stemming from this physical model is that the modes above the Boson peak are dispersive and intermediately localized. The dispersive character has been observed by INS experiments (Arai *et al* 1999a,b).

If the localized nature of the vibrational excitations continued well above the plateau region, the hopping of sl modes assisted by ex phonons might well be an important mechanism for thermal transport above the region of the rise of  $\kappa(T)$  proportional to  $T$  (see figure 34). This becomes quite possible because the local potential is soft and anharmonic, as verified by the pressure dependence of the RS (Hemley *et al* 1986) and INS experiments on the Debye–Waller factor (Nakamura *et al* 2002). The rise of  $\kappa(T)$  above the plateau proportional to  $T$  is quantitatively explained by the hopping mechanism assisted by ex acoustic phonons (Nakayama and Orbach 1999).

To sum up, the characteristic length scale  $R$  associated with the density fluctuation (local pressure fluctuation) due to the ring distribution plays a key role for the onset of localization of acoustic phonons at around 1 THz in  $v\text{-SiO}_2$ , and this leads to the plateau in the thermal conductivity. The local potentials stemming from randomly oriented buckled tetrahedra are responsible for the excess DOS, the Boson peak, which consists of sl modes owing to coupled rotations of  $\text{SiO}_4$  tetrahedra with optic mode nature. The modes above the Boson peak possess optic-mode nature as well, however, they are intermediately localized. This picture provides a consistent explanation for the thermal conductivity of  $v\text{-SiO}_2$  over the whole temperature range as well as the characteristic behaviours of  $S(Q, \omega)$  observed by INS experiments.

## Acknowledgments

The author is grateful to Professor O B Wright for a critical reading of the manuscript. This work was supported in part by a Grant-in-Aid from the Japan Ministry of Education, Science, and Culture.

## References

- Abrahams E, Anderson P W, Licciardello D C and Ramakrishnan 1979 *Phys. Rev. Lett.* **42** 690
- Ackerman D A and Anderson A C 1982 *Phys. Rev. Lett.* **49** 1176
- Akita Y and Ohtsuki T 1998 *J. Phys. Soc. Japan* **67** 2954
- Alexander S 1998 *Phys. Rep.* **296** 65
- Alexander S, Entin-Wohlman O and Orbach R 1986 *Phys. Rev. B* **34** 2726
- Anderson O L and Bömmel H E 1955 *J. Am. Ceram. Soc.* **38** 125
- Anderson P W, Halperin B I and Varma C M 1972 *Phil. Mag.* **25** 1
- Angell C A 1995 *Science* **267** 1924
- Aoki H, Syoho Y and Hemley R J 2000 *Physics Meets Mineralogy: Condensed Matter Physics in Geosciences* (Cambridge: Cambridge University Press)
- Arai M, Inamura Y, Otomo T, Kitamura N, Bennington S M and Hannon A C 1999a *Physica B* **263–264** 268
- Arai M, Inamura Y and Otomo T 1999b *Philos. Mag.* **B 79** 1733
- Arai T, Kataura H, Yasuoka H and Onari S 1985 *J. Non-Cryst. Solids* **77–78** 1149
- Arndt J 1969 *J. Am. Ceram. Soc.* **52** 285
- Arndt J 1983 *Phys. Chem. Glasses* **24** 104
- Bée M 1988 *Quasielastic Neutron Scattering* (Bristol: Hilger)
- Bell R J, Bird N F and Dean P 1968 *J. Phys. C* **1** 299
- Bell R J and Dean P 1972 *Philos. Mag.* **25** 1381
- Bennasi P, Krisch M, Masciovecchio C, Mazzacurati V, Monaco G, Ruocco G, Sette F and Verbeni R 1966 *Phys. Rev. Lett.* **77** 3835
- Bennasi P *et al* 1997 *Phys. Rev. Lett.* **77** 4670
- Berman R 1949 *Phys. Rev.* **76** 315
- Berman R 1950 *Proc. R. Soc. A* **208** 90
- Bernasconi A, Sleater T, Posselt D, Kjems J K and Ott H R 1992 *Phys. Rev. B* **45** 10363
- Bilar and Phillips W A 1975 *Philos. Mag.* **32** 113
- Binder K and Kob W 1998 *Analysis of Composition and Structure of Glass, and Glass Ceramics* ed H Bach and D Kranse (Berlin: Springer)
- Born M and Huang H 1954 *Dynamical Theory of Crystal Lattices* (Oxford: Oxford University Press)
- Bosworth D R, Hayes W, Spray A P L and Watkins G D 1970 *Proc. R. Soc. A* **317** 133
- Bridgman P W 1948 *Am. Acad. Arts. Sci.* **76** 55
- Brown K G *et al* 1972 *Proc. Nat. Acad. Sci. USA* **69** 1467
- Buchenau U 2001 *J. Phys.: Condens. Matter* **13** 7827
- Buchenau U, Nuecker N and Diamoux A J 1984 *Phys. Rev. Lett.* **53** 2316
- Buchenau U, Prager M, Nuecker N, Dianoux A J, Ahmad N and Phillips W A 1986 *Phys. Rev. B* **34** 5665
- Buchenau U, Zho H M, Nuecker N, Gilroy K S and Phillips W A 1988 *Phys. Rev. Lett.* **60** 1318
- Buchenau U, Wischniewski A, Nonkenbusch M and Schmidt W 1999 *Philos. Mag.* **B 79** 2021
- Cahill D G and Pohl R O 1987 *Phys. Rev. B* **35** 4067
- Cahill D G, Watson S K and Pohl R O 1992 *Phys. Rev. B* **46** 6131
- Caplin D, Gruener G and Dunlop J B 1973 *Phys. Rev. Lett.* **30** 1138
- Carpenter J M and Pelizzari C A 1975 *Phys. Rev. B* **12** 2391
- Carpenter J M and Price D L 1985 *Phys. Rev. Lett.* **54** 441
- Caruzzo H M, Grannan E R and Yu C C 1994 *Phys. Rev. B* **50** 6685
- Chervinka L 1987 *J. Non-Cryst. Solids* **92** 31
- Cusack S and Doster W 1990 *Biophys. J.* **58** 1990
- Cyvin S J, Rauch J E and Decius J C 1965 *J. Chem. Phys.* **43** 4083
- Debye P 1912 *Ann. Physik* **39** 788
- Dell'Anna R, Ruocco G, Sampoli M and Villani G 1998 *Phys. Rev. Lett.* **80** 1236
- Della Valle R G and Venutti E 1994 *Chem. Phys.* **179** 411
- Devine R A B, Dupree R, Farnan I and Capponi J J 1987 *Phys. Rev. B* **35** 2560
- Dove M T, Harris M J, Hannon A C, Parker J M, Swainson I P and Gambhir M 1997 *Phys. Rev. Lett.* **78** 1070
- Einstein A 1907 *Ann. Physik* **22** 180
- Elliott S R 1991 *Phys. Rev. Lett.* **67** 711
- Elliott S R 1992 *Europhys. Lett.* **19** 201
- Flubacher P, Leadbetter A J, Morrison J A and Stoicheff B P 1959 *J. Phys. Chem. Solids* **12** 53
- Foret M, Courtens E, Vacher R and Suck J B 1996 *Phys. Rev. Lett.* **77** 3831
- Foret M, Courtens E, Vacher R and Suck J B 1997 *Phys. Rev. Lett.* **78** 4669

- Foret M, Helen B, Taillade G, Cortens E, Vacher R, Casalta H and Dorner B 1998 *Phys. Rev. Lett.* **81** 2100
- Fowler T G and Elliott S R 1987 *J. Non-Cryst. Solids* **92** 31
- Freeman J J and Anderson A C 1986 *Phys. Rev. B* **34** 5684
- Galeener F L 1982 *J. Non-Cryst. Solids* **49** 53
- Galeener F L and Lucovsky G 1976 *Phys. Rev. Lett.* **29** 1474
- Galeener F L, Leadbetter A J and Stringfellow M W 1983 *Phys. Rev. B* **27** 1052
- Galeener F L and Mikkelsen J C Jr 1981 *Phys. Rev. B* **23** 5527
- Galeener F L and Geissberger A E 1983 *Phys. Rev. B* **27** 6199
- Galeener F L, Barrio R A, Martines E and Elliott R J 1984 *Phys. Rev. Lett.* **53** 2429
- Gaskell P H and Wallis D J 1996 *Phys. Rev. Lett.* **76** 66
- Genzel L *et al* 1976 *Biopolymers* **15** 219
- Gibbons D F 1959 *Phys. Chem. Solids* **11** 246
- Giddy A D, Dove M T, Pawley G S and Heine V 1993 *Acta Crystallogr. Sect. A* **49** 697
- Graebner J E, Golding B and Allen L C 1986 *Phys. Rev. B* **34** 5696
- Grannan E R, Randeria M and Sethna J P 1990 *Phys. Rev. B* **41** 7784
- Grannan E R, Randeria M and Sethna J P 1990 *Phys. Rev. B* **41** 7799
- Grimsditch M 1984 *Phys. Rev. Lett.* **52** 2379
- Guillot B and Guissani Y 1997 *Phys. Rev. Lett.* **78** 2401
- Guissani Y and Guillot B 1996 *J. Chem. Phys.* **104** 7633
- Hannon A C, Arai M, Sinclair R N and Wright A C 1992 *J. Non-Cryst. Solids* **150** 239
- Harris M J, Bennigton, Dove M T and Parker J M 1999 *Physica B*
- He H and Thorpe M F 1985 *Phys. Rev. Lett.* **54** 2107
- Helen B, Courtens E, Vacher R, Yamanaka A, Kataoka M and Inoue K 2000 *Phys. Rev. Lett.* **84** 5355
- Hemley R J, Mao H K, Bell P M and Mysen B O 1986 *Phys. Rev. Lett.* **57** 747
- Hemley R J, Meade C and Mao H K 1997 *Phys. Rev. Lett.* **79** 1420
- Horbach J, Kob W and Binder K 1998 *J. Non-Cryst. Solids* **235** 320
- Horbach J, Kob W and Binder K 1999 *J. Phys. Chem. B* **103** 4104
- Hunklinger S, Enss C and Strehlow S 1999 *Physica B* **263–264** 248
- Horbach J, Kob W and Binder K 2001 *Eur. Phys. J. B* **19** 531
- Inamura Y, Arai M, Yamamoto O, Inabe A, Kitamura N, Otomo T, Matusuo T, Bennington S M and Hannon A C 1998 *Physica B* **241–243** 903
- Inamura Y, Arai M, Yamamoto O, Inabe A, Kitamura N, Otomo T, Matsuo T, Bennington S M and Hannon A C 1999 *Physica B* **263–264** 299
- Inamura Y, Arai M, Otomo T, Kitamura N and Buchenau U 2000 *Physica B* **284–288** 1157
- Inamura Y, Arai M, Nakamura M, Otomo T, Kitamura N, Bennington S M, Hannon A C and Buchenau U 2001 *J. Non-Cryst. Solids* **293–295** 389
- Ioffe A F and Regel A R 1960 *Prog. Semicond.* **4** 237
- Jäckle J 1983 *Z. Phys. B-Condens. Matter* **52** 133
- John S, Sompolinsky H and Stephen M J 1983 *Phys. Rev. B* **27** 5592
- Kanaya K, Kaji K, Ikeda S and Inoue K 1988 *Chem. Phys. Lett.* **150** 334
- Karpov V G, Klinger M I and Ignatiev F N 1983 *Zh. Sov. Phys. JETP* **57** 439
- Karpov V G and Parshin D A 1985 *Soviet Phys. JETP* **61** 1308
- Keating P N 1966 *Phys. Rev.* **153** 774
- Keen D A and Dove M T 1999 *J. Phys.: Condens. Matter* **11** 9263
- Kettermann S, Fulde P and Strehlow P 1999 *Phys. Rev. Lett.* **83** 4325
- Khalatnikov I M 1952 *Zh. Eksp. Teor. Fiz.* **22** 687
- Kimizuka H, Kaburaki H and Kogure Y 2000 *Phys. Rev. Lett.* **84** 5548
- Kohara S and Suzuya K 2001 *Phys. Chem. Glasses* at press
- Krishnan R S 1953 *Proc. Indian Acad. Sci. A* **37** 377
- Lacks D J 1998 *Phys. Rev. Lett.* **80** 5385
- Lacks D J 2000 *Phys. Rev. Lett.* **84** 4629
- Landau L D and Lifshitz E M 1979 *Physical Kinetics* (Oxford: Pergamon) chapter 7
- Lassmann 1996 *Physica B* **219&220** 730
- Laughlin R B and Joannopoulos J D 1977 *Phys. Rev. B* **16** 2942
- Laughlin R B and Joannopoulos J D 1978 *Phys. Rev. B* **17** 2790
- Leadbetter A J 1969 *J. Chem. Phys.* **51** 779
- Le Bail A J 1995 *J. Non-Cryst. Solids* **185** 39
- Leyser H, Doster W and Diehl M 1999 *Phys. Rev. Lett.* **82** 2987

- Lovesey S W 1984 *Theory of Thermal Neutron Scattering* (Oxford: Clarendon)
- Ludwig S Enss C Strehlow P and Hunklinger S 2002 *Phys. Rev. Lett.* **88** 75501-1
- Marath C J and Maris H J 1996 *Phys. Rev. B* **54** 203
- Malinovsky V K, Novikov V N, Parshin P P, Sokolov A P and Zemlyanov M G 1990 *Europhys. Lett.* **11** 43
- Masciovecchio C *et al* 1997 *Phys. Rev. B* **55** 8049
- Masciovecchio C *et al* 1999 *Philos. Mag. B* **79** 2013
- Matsumoto D S, Reynolds C L and Anderson A C 1977 *Phys. Rev. B* **16** 3303
- Meade C, Hemley R J and Mao H K 1992 *Phys. Rev. Lett.* **69** 1387
- Mishima O, Calvert L D and Whalley E 1985 *Nature* **314** 76
- Moss S C and Price D L 1985 *Physics of Disordered Materials* ed D Adler, H Fritzsche and S R Ovshinsky (New York: Plenum) p 77
- Mott N F and Twose W P 1961 *Adv. Phys.* **10** 107
- Mozzi R L and Warren B E 1969 *J. Appl. Cryst.* **2** 164
- Mukherjee G D, Vaidya S N and Sugandhi V 2001 *Phys. Rev. Lett.* **87** 195501
- Nakamura M, Arai M, Otomo T, Inamura Y and Bennington S M 2001 *J. Non-Cryst. Solids* **293–295** 377
- Nakamura M, Arai M, Inamura Y and Otomo T 2002 *Phys. Rev. B* **66** 024203
- Nakayama T 1989 *Progress in Low Temperature Physics* vol XII, ed D F Brewer (Amsterdam: Elsevier) p 166
- Nakayama T 1998a *Phys. Rev. Lett.* **80** 1244
- Nakayama T 1999 *J. Phys. Soc. Japan* **68** 3540
- Nakayama T and Odajima A 1972 *J. Phys. Soc. Japan* **33** 12
- Nakayama T and Odajima A 1973 *J. Phys. Soc. Japan* **34** 732
- Nakayama T, Yakubo K and Orbach R 1994 *Rev. Mod. Phys.* **66** 381
- Nakayama T and Sato N 1998 *J. Phys.: Condens. Matter* **10** L41
- Nakayama T and Orbach R 1999 *Europhys. Lett.* **47** 468
- Nakayama T and Yakubo K 2001 *Phys. Rep.* **349** 239
- Neuefeind J Bunsenges K D 1996 *Phys. Chem.* **100** 1341
- Novikov V N and Sokolov A P 1991 *Solid State Commun.* **77** 243
- Ohsaka T and Oshikawa S 1998 *Phys. Rev. B* **57** 4995
- Ohsaka T, Shoji T and Tanaka K 2000 *J. Phys. Soc. Japan* **69** 3711
- Parshin D A 1994 *Phys. Solid State* **36** 991
- Pasquarello A 2000 *Phys. Rev. B* **61** 3951
- Pasquarello A and Car R 1998 *Phys. Rev. Lett.* **80** 5145
- Pasquarello A, Sarnthein J and Car R 1998 *Phys. Rev. B* **57** 14133
- Peierls R 1929 *Ann. Phys. (Leipzig)* **3** 1055
- Phillips J C 1981 *J. Non-Cryst. Solids* **43** 37
- Phillips W A 1972 *J. Low Temp. Phys.* **7** 1657
- Phillips W A 1987 *Rep. Prog. Phys.* **50** 1657
- Pilla O, Gunsolo A, Fontana A, Masciovecchio C, Montagna M, Puocco G, Scopigno T and Sette F 2000 *Phys. Rev. Lett.* **85** 2136
- Pluth J J, Smith J V and Faber J Jr 1985 *J. Appl. Phys.* **57** 1045
- Pohl R O 1981 *Amorphous Solids: Low Temperature Properties* ed W A Phillips (Berlin: Springer) p 27
- Polian A and Grimsditch M 1990 *Phys. Rev. B* **41** 6086
- Price D L and Carpenter J M 1987 *J. Non-Cryst. Solids* **92** 153
- Rat E Foret, M Courtens, E Vacher R and Arai M 1999 *Phys. Rev. Lett.* **83** 1355
- Rogge S, Natelson D and Osheroff D D 1996 *Phys. Rev. Lett.* **76** 3136
- Rogge S, Natelson D, Tiger B and Osheroff D D 1997a *Phys. Rev. B* **55** 11256
- Rogge S, Natelson D and Osheroff D D 1997b *J. Low Temp. Phys.* **106** 717
- Rothenfusser M, Dietsche W and Kinder H 1984 *Phonon Scattering in Condensed Matter* ed W Eisenmenger *et al* (Berlin: Springer) p 419
- Ruocco G and Sette F 2001 *J. Phys.: Condens. Matter* **13** 9141
- Salce B and Boatner L A 1986 *Phonon Scattering in Condensed Matter V* (Berlin: Springer) p 272
- Sarnthein J, Pasquarello A and Car R 1995a *Phys. Rev. Lett.* **74** 4682
- Sarnthein J, Pasquarello A and Car R 1995b *Phys. Rev. B* **52** 12690
- Sarnthein J, Pasquarello A and Car R 1997 *Science* **275** 1925
- Schirmacher W 1998 *Phys. Rev. Lett.* **81** 136
- Schulze H 1990 *Glass: Nature, Structure and Properties* (Heidelberg: Springer)
- Scopigno T, D'astuto M, Krish M, Ruocco G and Sette F 2001 *Phys. Rev. B* **64** 012301-1
- Sen P and Thorpe 1977 *Phys. Rev. B* **15** 4030

- Simons S 1964 *Proc. Phys. Soc.* **83** 749
- Sinclair R N, Erwin-Desa J A, Etherington G, Johnson P A V and Wright A C 1980 *J. Non-Cryst. Solids* **42** 107
- Sokolov A P, Kislink A, Soltwisch M and Quitmann D 1992 *Phys. Rev. Lett.* **69** 1540
- Sokolov A P, Calemczuk R, Salce B, Kisliuk A, Quitmann D and Duval E 1993 *Phys. Rev. B* **48** 7692
- Sokolov A P, Calemczuk R, Salce B, Kisliuk A, Quitmann D and Duval E 1997 *Phys. Rev. Lett.* **78** 2405
- Squires G L 1984 *Introduction to the Theory of Neutron Scattering* (London: Cambridge University Press)
- Stone C E *et al* 2001 *J. Non-Cryst. Solids* **293–295** 769
- Strehlow P, Enss C and Hunklinger S 1998 *Phys. Rev. Lett.* **80** 5361
- Sugai S and Onodera A 1996 *Phys. Rev. Lett.* **77** 4210
- Susman S *et al* 1991 *Phys. Rev. B* **43** 1194
- Suzuya K, Kohara S, Yoneda Y and Umesaki N 2000 *Phys. Chem. Glasses* **41** 282
- Suzuya K, Shibata K, Umesaki N, Kitamura N and Kohara S 2001 *J. Phys. Soc. Jpn. Suppl. A* **70** 256
- Swainson I P and Dove M T 1993 *Phys. Rev. Lett.* **71** 193
- Swainson I P and Dove M T 1995 *J. Phys.: Condens. Matter* **7** 1771
- Taraskin S N and Elliott S R 1997a *Phys. Rev. B* **56** 8605
- Taraskin S N and Elliott S R 1997b *Europhys. Lett.* **39** 37
- Taraskin S N and Elliott S R 1998 *Philos. Mag. B* **77** 403
- Taraskin S N and Elliott S R 2000 *Phys. Rev. B* **61** 12031
- Thorpe M F 1983 *J. Non-Cryst. Solids* **57** 355
- Trachenko K, Dove M T, Hammonds K O, Harris M J and Heine V 1998 *Phys. Rev. Lett.* **81** 3431
- Trachenko K, Dove M T, Harris M J and Heine V 2000 *J. Phys.: Condens. Matter* **12** 8041
- Treloar L R 1975 *The Physics of Rubber Elasticity* (Oxford: Clarendon)
- Tsuneyuki S, Tsukada M, Aoki H and Matsui Y 1988 *Phys. Rev. Lett.* **61** 869
- Tucker M G, Squires M P, Dove M T and Keen D A 2001 *J. Phys.: Condens. Matter* **13** 403
- Uchino T, Tokuda Y and Yoko T 1998 *Phys. Rev. B* **58** 5322
- Uchino T, Kitagawa Y and Yoko T 2000 *Phys. Rev. B* **61** 234
- Vacher R, Pelous J, Plicque F and Zarembowitch A 1981 *J. Non-Cryst. Solids* **45** 397
- Vacher R, Pelous J and Courtens E 1997 *Phys. Rev. B* **56** R481
- Vacher R, Foret M, Courtens E, Pelous J and Suck J-B 1998 *Philos. Mag. B* **77** 523
- Vacher R, Courtens E and Foret M 1999 *Philos. Mag. B* **79** 1763
- van Beest B W H, Kramer G J and Santen R A 1990 *Phys. Rev. Lett.* **64** 1955
- von Löhneysen H, Ruesing H and Sander W 1985 *Z. Phys. B* **60** 323
- Vollmayr K, Kob W and Binder K 1996 *Phys. Rev. B* **54** 15808
- Vukcevich M R 1972 *J. Non-Cryst. Solids* **11** 25
- Winterling G 1975 *Phys. Rev. B* **12** 2432
- Wischniewski A, Buchenau U, Dianoux A J, Kamitakahara W A and Zarestky J L 1998 *Philos. Mag. B* **77** 579
- Wohlfahrt M, Strehlow P, Enss C and Hunklinger S 2001 *Europhys. Lett.* **56** 690
- Wright A C, Sinclair R N and Leadbetter A J 1985 *J. Non-Cryst. Solids* **71** 295
- Wright A C *et al* 1991 *J. Non-Cryst. Solids* **129** 213
- Wright O B and Phillips W A 1984 *Philos. Mag.* **50** 63
- Würger A 2002 *Phys. Rev. Lett.* **88** 75502-1
- Yakubo K and Nakayama T 1987 *Phys. Rev. B* **30** 8933
- Yamada-Kaneda H, Kaneda C and Ogawa T 1993 *Phys. Rev. B* **47** 9338
- Yamaguchi M, Nakayama T and Yagi T 1998 *Physica B* **263–264** 258
- Yamaguchi M and Yagi T 1999a *Europhys. Lett.* **47** 462
- Yamaguchi M and Yagi T 1999b *Conf. Proc. Phys. Soc. Japan* p 894
- Yu C C and Leggett A J 1988 *Comments Condens. Matter Phys.* **14** 231
- Zeller R C and Pohl R O 1971 *Phys. Rev. B* **4** 2029
- Zaitlin M P and Anderson A C 1975 *Phys. Rev. B* **12** 4475
- Zhu T C, Maris H J and Tauc J 1991 *Phys. Rev. B* **44** 4281
- Zhu D-M 1994 *Phys. Rev. B* **50** 6053